Geomorphology 511 (2026) 110445

Contents lists available at ScienceDirect

Geomorphology

journal homepage: www.journals.elsevier.com/geomorphology

Factors controlling asymmetry in submarine channels and submarine canyons: Insights from global morphological analysis

Nadezhda Lagunova [a,b,*], Tilmann Schwenk [b], Michael A. Clare [c], Ricardo Silva Jacinto [d], Dierk Hebbeln [a,b], Volkhard Spieß [b], Gerhard Bohrmann [a,b], Pelle H. Adema [e], Joris T. Eggenhuisen [e], Elda Miramontes [a,b]

[a] MARUM-Center for Marine Environmental Sciences, University of Bremen, Bremen, 28359, Germany
[b] Faculty of Geosciences, University of Bremen, Bremen, 28359, Germany
[c] National Oceanography Centre, European Way, Southampton, SO14 3HZ, UK
[d] Ifremer, Geo-Ocean, UMR 6538, Plouzané, 29280, France
[e] Faculty of Geosciences, Utrecht University, Utrecht, 3584 CB, Netherlands

ARTICLE INFO

Keywords:
Turbidity currents
Asymmetric submarine channels
Canyons
Levee asymmetry
Width asymmetry
Mixed turbidite-contourite systems
Gravity flows
Bottom currents
Coriolis force

ABSTRACT

The formation of asymmetric submarine channels and canyons is the result of multiple processes, including bottom currents, Coriolis forcing, and centrifugal forces, acting on turbidity flows. Despite increasing studies of asymmetric submarine canyons and channels and recognition of the influence of bottom currents on turbidity flows, the relative contributions of these factors remain poorly constrained, often resulting in contradictory interpretations. In this study, we investigate whether morphometric characteristics of submarine canyons and channels – specifically relief and width asymmetries, and cross-sectional slope angles – can indicate the most likely processes responsible for their asymmetry, such as Coriolis effect versus bottom currents. We systematically analysed 24 asymmetric canyons and channels from diverse settings, integrating their morphometric data with environmental parameters including latitude, water depth, slope angle, and bottom current intensity and direction.

Our results reveal substantial variability in channel asymmetry along their lengths: the positions of the higher margin, thalweg, steeper margin, and the degree of asymmetry often change within a system, so that a single channel cannot be consistently described with one asymmetry value. Depth-dependent variations in slope, water-mass structure, turbidity current dynamics, and bottom-current intensity, combined with temporal variability in both turbidity-current characteristics and bottom-current velocities, create locally coherent, but non-predictive asymmetry. Thus, our observations suggest that morphological characteristics alone are insufficient to identify the main forces controlling channel asymmetry. We propose a classification scheme to aid interpretation of channel asymmetry and potential bottom current interactions, emphasizing the complexity of channel formation.

1. Introduction

Turbidity currents are high-energy, gravity-driven submarine flows that transport vast amounts of sediments from the continental shelf and shallow environments to the deep sea (Covault et al., 2012; Talling, 2014). These currents play a major role in the transfer of terrigenous carbon to the deep sea (Talling et al., 2024), can efficiently transport nutrients and pollutants to deep-marine environments (Chen et al., 2025; Fontanier et al., 2012; Khripounoff et al., 2012), and can pose a hazard for seafloor infrastructure (Carter et al., 2014).

Gravity flows typically exhibit vertical stratification in sediment composition, concentration and velocity (Amy et al., 2005; Kneller and Buckee, 2000). The basal, more concentrated, portion of the flow, dominated by coarser and denser particles, often erodes and incises the seafloor, contributing to the development of channelized features, named submarine canyons and submarine channels (Kneller and Buckee, 2000). However, submarine channels may also develop through aggradation without significant incision (Stevenson et al., 2013). The upper part of the flow is more dilute and generally composed of finer particles that travel slower and are more prone to

* Corresponding author at: MARUM-Center for Marine Environmental Sciences, University of Bremen, Bremen, 28359, Germany.
E-mail address: lagunova@uni-bremen.de (N. Lagunova).

https://doi.org/10.1016/j.geomorph.2026.110445
Received 8 December 2025; Received in revised form 18 June 2026; Accepted 4 July 2026
Available online 7 July 2026

lateral deposition along the margins of submarine channels, leading to the formation of levees (Kneller, 1995).

It is well known that factors like centrifugal and Coriolis forces strongly control channel asymmetry. As in fluvial systems, centrifugal force affects the flow structure and channel shape in submarine channels at their bends (Komar, 1969; Imran et al., 1999). Subsequently, the role of Coriolis forces – particularly evident at higher latitudes – was recognized as another important control on levee asymmetry (Komar, 1969; Imran et al., 1999; Cossu et al., 2010).

Historically, contour currents had been considered too weak to significantly influence turbidity flows. Turbidity currents are short-lived but highly energetic, whereas bottom currents are persistent yet relatively slow (Rebesco et al., 2014). The number of studies indicating the presence of mixed turbidite-contourite systems has strongly increased since the early 2000s (Rodrigues et al., 2022b). It has been suggested that particularly the upper part of the flow can be entrained by bottom currents flowing along-slope, resulting in the formation of asymmetric channel-levee systems and mixed turbidite-contourite systems (Fonnesu et al., 2020; Miramontes et al., 2020, 2021; Rodrigues et al., 2022a,b).

Recent experimental work has begun to provide insight into the physical mechanisms of this interaction. In particular, flume experiments by Adema et al. (2025a) demonstrate that bottom currents can laterally deflect the velocity core of turbidity currents and modify their internal structure. Such deflection may be expressed in channel morphology, for example in the position of the thalweg or a steeper channel flank.

Despite growing interest in the interaction between gravity flows and bottom currents, it remains unclear how Coriolis force, centrifugal force, and bottom currents collectively influence channel morphology, including relief asymmetry and thalweg position. A major open question is whether it is possible to isolate their individual contributions to the observed channel asymmetry and to interpret the direction of bottom currents based on channel asymmetry and morphology. To answer this research question, we analysed the morphometric parameters of 24 submarine channels and canyons (levee asymmetry, width asymmetry, thalweg position and the slope angle of a channel margin), as well as their environmental parameters (latitude, water depth, slope angle and bottom current velocity).

2. Materials and methods

Morphological parameters of 24 asymmetric submarine channels and canyons from 15 different locations around the world (Fig. 1) were systematically measured based on bathymetric data. The dataset was compiled based on evidence of asymmetry, availability of suitable bathymetric data, and sufficient spatial coverage for analysis, and was designed to include a range of channel types and settings rather than represent a statistically complete global sample. We use the term 'channel' as a general definition for elongate, continuous downslope-oriented depressions on the seabed that are mainly formed by gravity-driven processes, which would include for instance submarine canyons (e.g., Portimão canyon, number 7 in Fig. 1; Marchès et al., 2007), valleys (e.g., Var, number 9 in Fig. 1; Migeon et al., 2000) and submarine channels (e.g., Nova Scotia, number 2 in Fig. 1; Normandeau et al., 2019). Although submarine canyons and submarine channels differ in their formative processes and morphology (e.g., Harris and Whiteway, 2011), the transition between these end-members is often gradual and not readily delineated. For instance, Harris and Whiteway (2011) classified systems with incision exceeding 100 m as submarine canyons, however, some channel-levee systems can exhibit reliefs greater than 100 m while not fitting the geomorphological definition of canyons (e.g., Bounty channel). Broader or alternative terminology has also been used in the literature (e.g., 'conduits' in Allen et al., 2022; 'bathymetric lows' in Nanson et al., 2026), however these terms refer either to process-based concepts or to a broader range of seabed features than considered here. The term 'channel' is therefore used here in a broad sense to include features that may also be classified as canyons or valleys in other contexts. We follow the common nomenclature for the different systems based on previous literature when it is already well established, therefore some of the depressions are named channel (e.g., Bounty channel; Carter and Carter, 1987, 1996; Deng et al., 2024), while others are named canyon (e.g., Portimão canyon; Marchès et al., 2007, 2010; Mulder et al., 2006). Information on the source and spatial resolution of bathymetric maps used for each channel is provided in Table 1.

2.1. Morphological parameters description

The measured morphological parameters of channels include relief, width, relief symmetry and width symmetry, slope angle of the channel margins, global and local sinuosity, downslope angle and water depth along thalweg. We define relief as the maximum vertical distance between the thalweg and the channel margin (Shumaker et al., 2018). A channel margin is identified as the levee crest, or, in the absence of a clearly defined levee, as the rollover point (Shumaker et al., 2018) (Fig. 2A). Left ($Relief_L$) and right ($Relief_R$) relief refer to the vertical distance from the thalweg to the left and right margins, respectively.

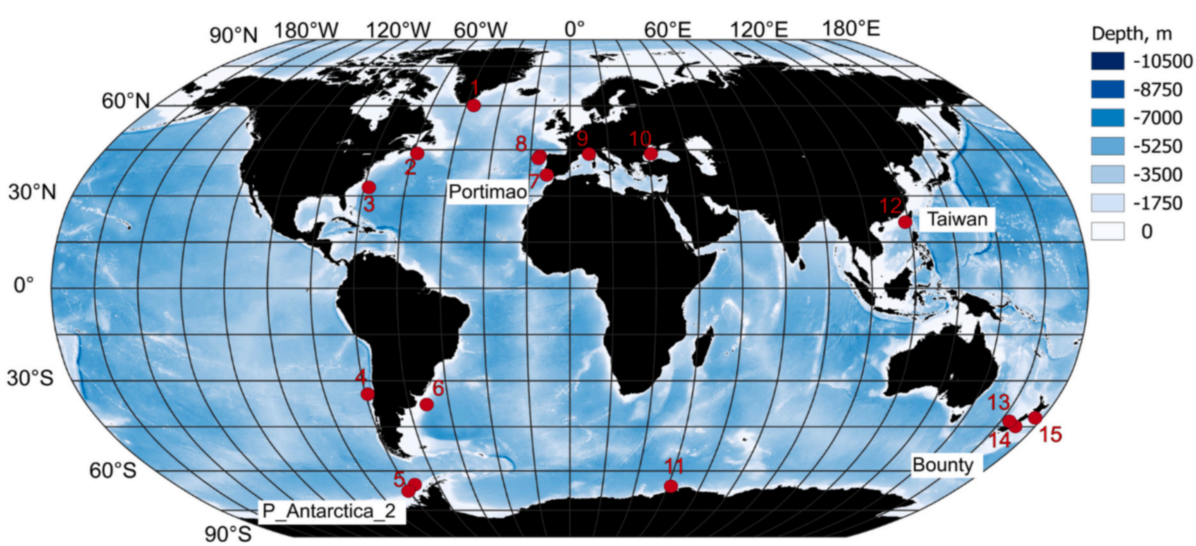

Fig. 1. Locations of the studied channels shown on a global map (see Table 1 for channel details). The name of the channels shown in more detail in this study is indicated on the map.

Table 1
Study locations, channel names, source and resolution of bathymetric maps, source of bottom current models, and water depth ranges and temporal extent of the models.

Number	Location	Channels	Bathymetry source	Resolution of the bathymetry	Bottom currents model	Depth	Spatial resolution of bottom currents model	Time for averaging bottom currents data	Previous studies
1	Northwest Mediterranean Sea	Var	EMODnet	24 × 24 m	Escudier et al., 2020	1500–2500 m	0.042° × 0.042°	Monthly 01.01.1987–01.07.2025	Migeon et al. (2000), Mas et al. (2010), Khripounoff et al. (2012), Payo Payo (2016)
2	South China Sea	Taiwan	Wintersteller and Kramer (2019)	100 × 100 m (resampled from 25 × 25 m)	Copernicus Marine Service, 2016	2000–2000 m	Approx. 8 km	Monthly 01.01.1993–01.06.2021	Li et al. (2021), Xu et al. (2014)
3	Nova Scotia Margin, Northwest of Canada	Nova_Scotia Shortland_Haldimand	GEBCO 2023	386 × 386 m		3800–5500 m			Normandeau et al. (2019)
4	Galicia Bank region, northwest Iberia	Galicia_NE Galicia_S	EMODnet	101 × 101 m	Copernicus Marine Service, 2017	1800–4000 m	0.028° × 0.028°	Monthly 01.12.2022–01.05.2025	Ercilla et al. (2011)
5	Hatteras Outer Ridge, Atlantic margin of the USA	Hatteras	NCEI	82 × 82 m	Copernicus Marine Service, 2016	3000–5500 m	Approx. 8 km	Monthly 01.01.1993–01.06.2021	Gardner et al. (2016)
6	Canterbury Basin, Southeast of New Zealand	Bounty	NIWA New Zealand bathymetric grid 2016	250 × 250 m		1000–4000 m			Carter and Carter (1988, 1996), Horn and Uenzelmann-Neben (2015)
7	East Coas Basin, Northeast of New Zealand	Hikurangi				2500–4500 m			Lewis et al. (1998)
8	Challenger Plateau basins, Southwest of New Zealand	Hokitika				2200–4200			Neil et al. (2015)
9	Black Sea	Danube	Wintersteller and Klaucke (2016)	125 × 125 m	Copernicus Marine Service, 2025	800–1700 m	0.025° × 0.025°	Monthly 01.01.1993–01.12.2023	Stanev (2005), Popescu et al. (2001)
10	South and southeast of Greenland	S_Greenland_1 S_Greenland_2 SE_Greenland	IBCAO	200 × 200 m	Copernicus Marine Service, 2015	1000–3500 m 1000–2500 m	6.25 × 6.25 km	Monthly 05.07.2021–07.08.2025	Rasmussen et al. (2003)
11	West of Argentina	Mar_del_Plata	Warnke et al. (2023)	102 × 102 m	Copernicus Marine Service, 2016	1000–3500 m	Approx. 8 km	Monthly 01.01.1993–01.06.2021	Warratz et al. (2019)
12	Southwest of Portugal	Portimão Portimão_C1 Portimão_C2 Portimão_C3	EMODnet	103 × 103 m	Copernicus Marine Service, 2017	1–3000 m	0.028° × 0.028°	Monthly 01.12.2022–01.05.2025	Marchès et al. (2007)
13	Offshore Chile	Biobio	GEBCO 2024	200 × 200 m	Copernicus Marine Service, 2016	0–4000 m	Approx. 8 km	Monthly 01.01.1993–01.06.2021	Bernhardt et al. (2015)
14	Cosmonaut Sea	Antarctica_Amundsen	IBSCO	500 × 500 m		2800–4800 m			Kuvaas et al. (2005)
15	Pacific Margin of the Antarctic Peninsula	P_Antarctica_1 P_Antarctica_2 P_Antarctica_3				2000–4000 m			Rebesco et al. (1996), Rodrigues et al. (2022a)

Channel sides (left and right) are defined in the downstream direction of the flow (i.e., looking downslope from the channel head).

Various approaches exist for measuring the width of submarine channels (Fierens et al., 2019; Konsoer et al., 2013; Reimchen et al., 2016; Palm et al., 2021). In this study, we define channel width as the horizontal distance between the left and right margin along lines orthogonal to the thalweg, following the approach of Konsoer et al. (2013). The position of the thalweg within the channel is described by the left ($Width_L$) and right ($Width_R$) components of the width, defined as the horizontal distances from the thalweg to the respective channel

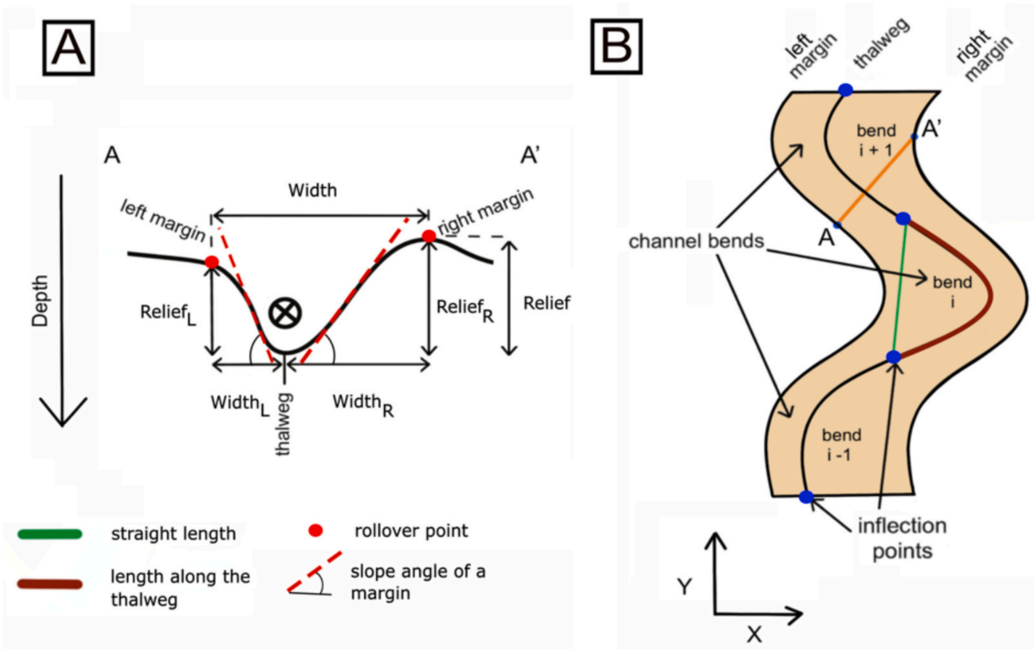

Fig. 2. Schematic illustration of the principles for measuring channel morphological parameters: A) Key morphological parameters assessed in this study; B) Concept of local sinuosity measurement and the position of the cross-section illustrated in (A). Cross-sections are oriented orthogonally to the local thalweg and may therefore be oblique to the channel margins.

margin (Fig. 2A).

To quantify channel asymmetry, we use two parameters: relief symmetry and width symmetry, which represent both the degree and direction of asymmetry. These parameters are expressed as symmetry indices (i.e., inverse measures of asymmetry), such that lower values correspond to more asymmetric channel geometries. Relief symmetry indicates which margin is higher, and by how much, relative to each other. Previous studies calculated relief asymmetry as the ratio between the maximum and minimum reliefs (Allen et al., 2022). We adapt this approach by introducing a sign to the ratio, indicating the side of the higher margin, and propose naming the signed metric relief symmetry (1).

$$\text{Relief symmetry} = \min(\text{Relief}_L, \text{Relief}_R)/(\max(\text{Relief}_L, \text{Relief}_R) \times \text{sign}(\text{Relief}_R - \text{Relief}_L) \quad (1)$$

Positive values indicate that the right margin is higher, while negative values indicate that the left margin is higher. Relief symmetry ranges from -1 to 1, with an absolute value of 1 representing an ideally symmetrical channel and values closer to 0 indicating greater asymmetry.

The position of the thalweg relative to the channel margins is captured by the width symmetry parameter, following a modified version of the method by Reimchen et al. (2016) (2). Width symmetry equals ±0.5 when the thalweg is located precisely in the middle between the two margins. Values lower than ±0.5 indicate that the thalweg is offset toward one side. The sign in formula (2) reflects the position of the thalweg relative to channel margins. For example, let Width_L be 4 and Width_R – 6. Since $\text{Width}_R > \text{Width}_L$, the thalweg is closer to the left margin and the difference Width_L - $\text{Width}_R = -2$ is negative (Fig. 2A):

$$\text{Width symmetry} = \min(\text{Width}_L, \text{Width}_R)/\text{Total Width} \times \text{sign}(\text{Width}_L - \text{Width}_R) \quad (2)$$

Global sinuosity was measured as the ratio between the channel length along the thalweg and straight-line distance from the channel head to its mouth (Shumaker et al., 2018). To capture sinuosity variations along the channel, we additionally calculated local sinuosity at each individual channel bend (Fig. 2B).

Several methods have been proposed to measure local sinuosity. Allen et al. (2022) and Hansen et al. (2017) calculated sinuosity within a sliding window of fixed length, with Allen et al. (2022) incorporating overlapping windows. Alternatively, Hasenhündl and Blanckaert (2022) suggested delineating channel loops by measuring sinuosity between inflection points – defined as the zero crossing of curvature along the channel centreline (Fig. 2B). In their method, the centreline is derived from the channel margins. However, margins of the channels analysed in this study do not always present the same sinuous pattern as the thalweg. Therefore, we opted to use a smoothed thalweg instead of a centreline, applying a Savitzky-Golay filter (Savitzky, 1964; Virtanen et al., 2020) to reduce noise while preserving larger-scale directional trends. Local sinuosity is then calculated for individual channel bends, defined between successive inflection points along the smoothed thalweg.

The along-channel length was computed based on the smoothed thalweg to avoid artificial inflation of sinuosity values due to minor direction fluctuations. Local sinuosity was then assigned along the channel path, with each value corresponding to the segment between two inflection points (i.e., a loop).

To further refine the results, the thalweg was resampled after smoothing to remove unintended self-intersections caused by small-scale directional variations not associated with true loops. Both filtering and resampling involved a degree of subjectivity, aiming to balance the removal of minor fluctuations with the preservation of meaningful channel bends.

Local sinuosity was calculated using the following expression:

$$\text{local sinuosity}_i = \text{length along the smoothed thalweg}_i/\text{straight length}_i, \quad (3)$$

where i denotes the index of a channel bend.

Downstream slope angle along thalweg was calculated using a sliding window approach, with the window size typically set to one-tenth of the total measured length, chosen to ensure scale-dependent smoothing of the longitudinal profile. In a few cases, slight adjustments to the window size were made to account for data resolution and local morphological characteristics. Depending on the scale and variability of the seafloor morphology, window lengths ranged from 1 to 100 km. We define the slope angle of a margin as the angle of the steepest and stable bank segment, excluding the channel bed and immediate proximity of the margin point, where slope angles are typically unstable (Fig. 2A). In cross-sections with a clearly defined flat zone, the beginning of slope was marked at the point where the slope starts to rise. In U-shaped channels, the beginning was identified at the location where the slope angle becomes relatively stable following a gradual, continuous incline.

2.2. Morphological parameters extraction

A Python script was developed to enable consistent and automated extraction of morphological parameters from submarine channels (Lagunova, 2026). The workflow consists of three main steps: (1) extraction of the thalweg and margin lines, (2) generation of cross-sections along the thalweg, followed by (3) calculation of morphological parameters for each cross-section. These cross-sections serve as the primary data points for subsequent morphometric analysis. The script requires three input datasets: a digital elevation model, a topographic position index (TPI) grid, and a polygon delineating the extent of the channel (Fig. 3).

Thalweg extraction was performed on bathymetric maps by consecutively identifying the minimum elevation within horizontally oriented slices taken along a fixed vertical axis in map view. This axis does not follow the exact curvature of the channel, but is aligned with the longest dimension of the predefined polygon, thereby approximating the overall trend of the channel (Fig. 3A). To reduce the risk of the extraction process shifting onto nearby channels or unrelated morphological features such as seamounts, a manually defined polygon was used to constrain the analysis to the main path of the target channel.

The topographic position index (TPI) was then used to delineate channel features. TPI quantifies the elevation of each point relative to its surrounding neighbourhood, defined by a specified radius (Weiss, 2001). Positive TPI values indicate locations that are higher than their surroundings – such as ridges or levees – making TPI particularly useful for identifying channel margins. TPI maps were generated using the QGIS Terrain Shading plugin (Čučković, 2025), and the radius used for TPI computation was selected based on a representative cross-section. Specifically, the radius was set to match the characteristic cross-channel scale, defined as the approximate pixel distance between the thalweg and the farthest channel margin, ensuring that the TPI window captures channel-margin morphology rather than broader background topography or small-scale features (e.g., a radius of 10 pixels for a ~4 km-wide channel with 386 m pixel size in the Shortland-Haldimand channel). The start and end point of the thalweg were defined by manually setting minimum and maximum TPI threshold values. For channels margins, two TPI threshold values were applied – one for the left and one for the right margin – to consistently capture their positions. Channel margins were then identified on TPI maps by locating maximum TPI values to the left and right of the thalweg within each horizontal slice (Fig. 3B), where the maximum TPI within the specified search window corresponds to the channel margin. In cases where levees are not present, these maxima correspond to rollover points, ensuring a consistent, algorithm-based definition of channel margins across all systems.

To reduce the influence of small-scale topographic variations and improve the continuity of the extracted thalweg and margin lines, sliding windows were applied during line tracking. Additionally, the extracted lines were commonly smoothed using a Savitzky-Golay filter (Savitzky, 1964; Virtanen et al., 2020).

The line extraction was performed on a two-dimensional array containing only depth values. To enable geographic mapping and visualization, the extracted thalweg and margin lines were subsequently transformed into geographical coordinates. Cross-sections were then generated at regular intervals along the thalweg, oriented perpendicular to the thalweg path. The spacing of cross-sections was defined individually for each system based on thalweg length, resulting in a scale-dependent sampling density that ensures adequate spatial coverage while maintaining computational feasibility for large systems (e.g., 500 m for a 10 km-long systems and 3 km for a 1100 km long system). However, cross-sections were only generated where both channel margins were successfully identified along a line perpendicular to the thalweg, resulting in a geometry-constrained rather than strictly evenly

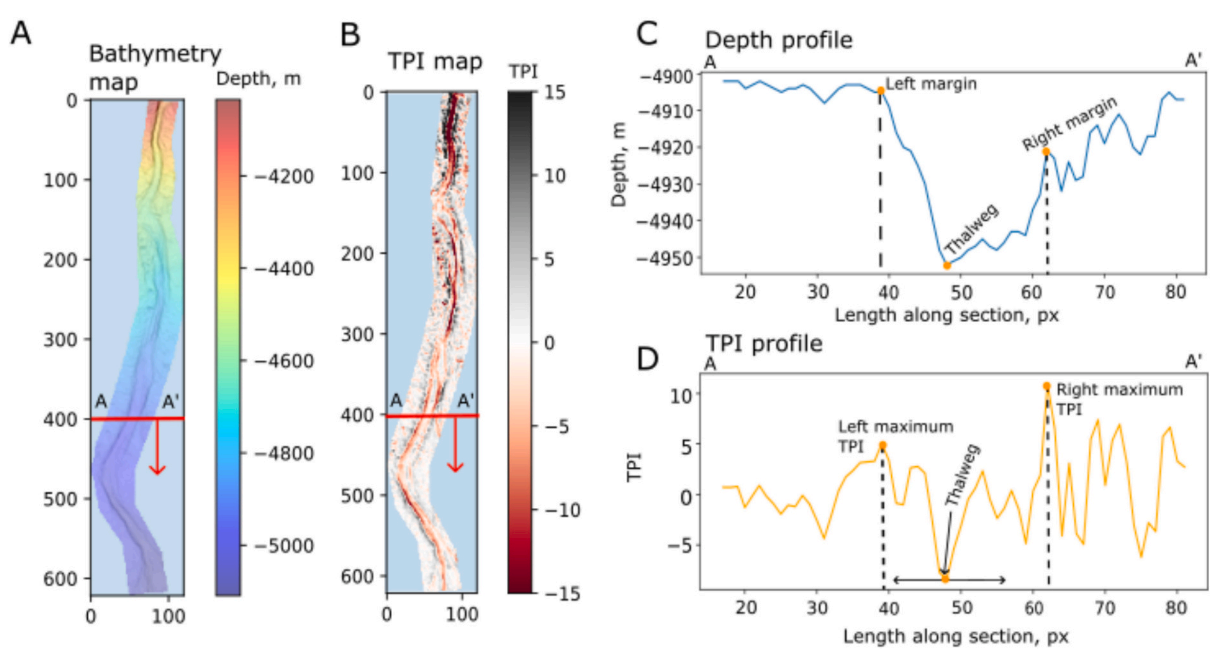

Fig. 3. Principles of automatic extraction of thalweg and margins lines: A) Bathymetry map constrained by a polygon (in this case for illustration the Shortland-Haldimand channel), with a moving AA′ transect illustrating the minimum bathymetry search for the thalweg at each position of AA′; B) Topographic Position Index (TPI) map calculated with a radius of 10 pixels (~4 km in this case); C) Depth profile along transect AA′ with the locations of thalweg, left and right margins; D) TPI profile along transect AA′, with locations of maximum TPI values on both sides of the thalweg, corresponding to the position of the margins.

spaced sampling scheme. In cases where the thalweg is partially decoupled from the channel margins (e.g., in some canyons systems), cross-sections may locally be oblique relative to the margins. At each generated cross-section, key morphometric parameters were automatically calculated, including channel width, channel relief, left and right margin reliefs, left and right width, width symmetry, relief symmetry, latitude, water depth, slope angle, and local sinuosity.

2.3. Characterisation of bottom currents at identified channel locations

Eastward and northward seawater velocity components were extracted for each channel using E. U. Copernicus Marine Service Information oceanographic reanalysis datasets (Copernicus Marine Service, 2015, 2016, 2017, 2025; Escudier et al., 2020). While the Global Ocean Physics Reanalysis was used in most cases, higher-resolution regional models were preferred when available to better capture local current dynamics (Table 1). These datasets used in this study typically provide monthly records spanning from January 1993 to June 2021 and include multiple depth layers, depending on the depth range of each channel (e.g., 2000–4000 m for the Taiwan canyon). The resulting velocity fields were spatially constrained using the same manually defined polygons applied in the morphological analysis, ensuring that current

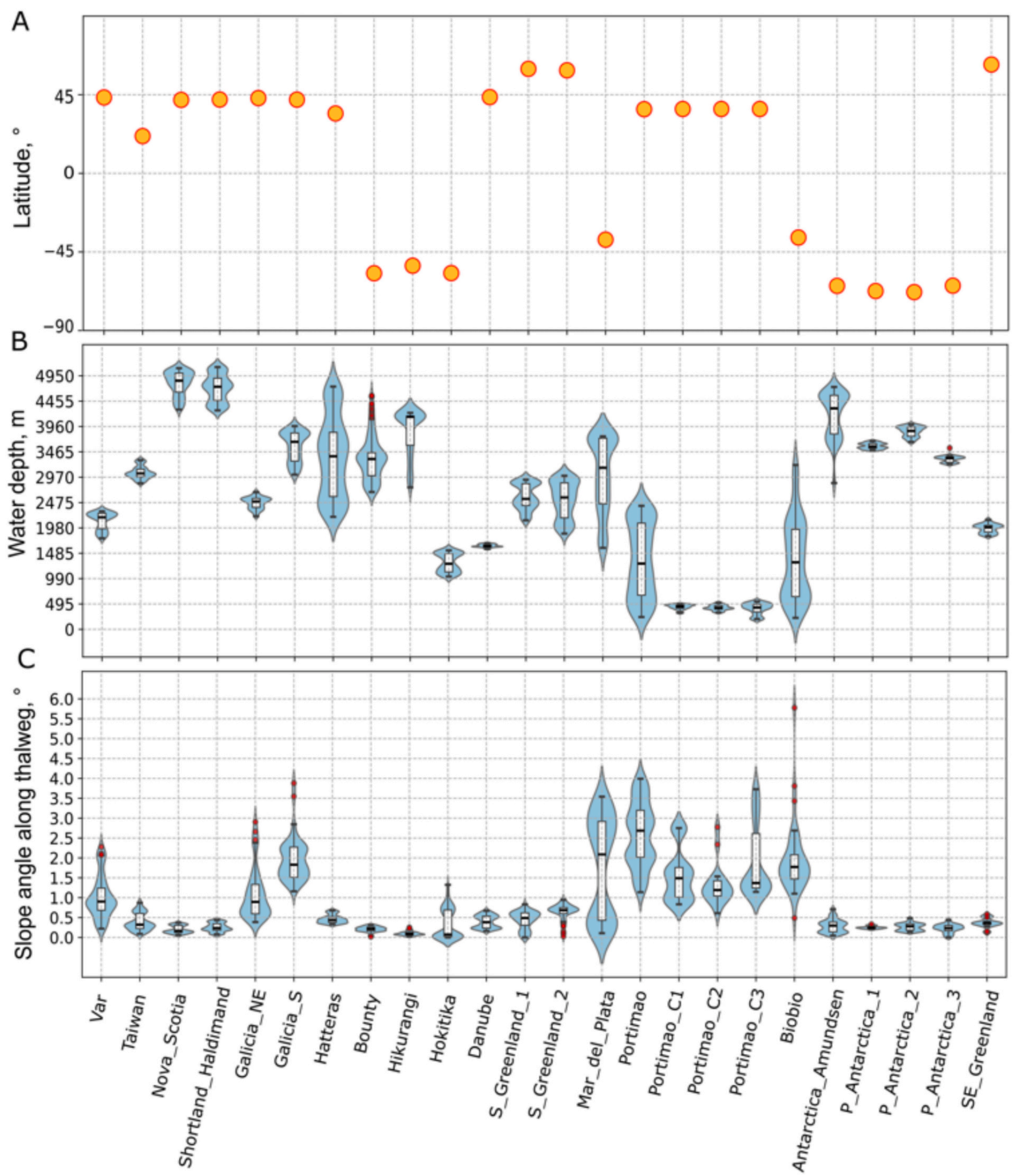

Fig. 4. Statistical distributions of environmental parameters for the 24 measured channels: A) Latitude; B) Water depth; and C) Slope angle along thalweg, represented as violin plots overlaid with boxplots, with red dots corresponding to outliers.

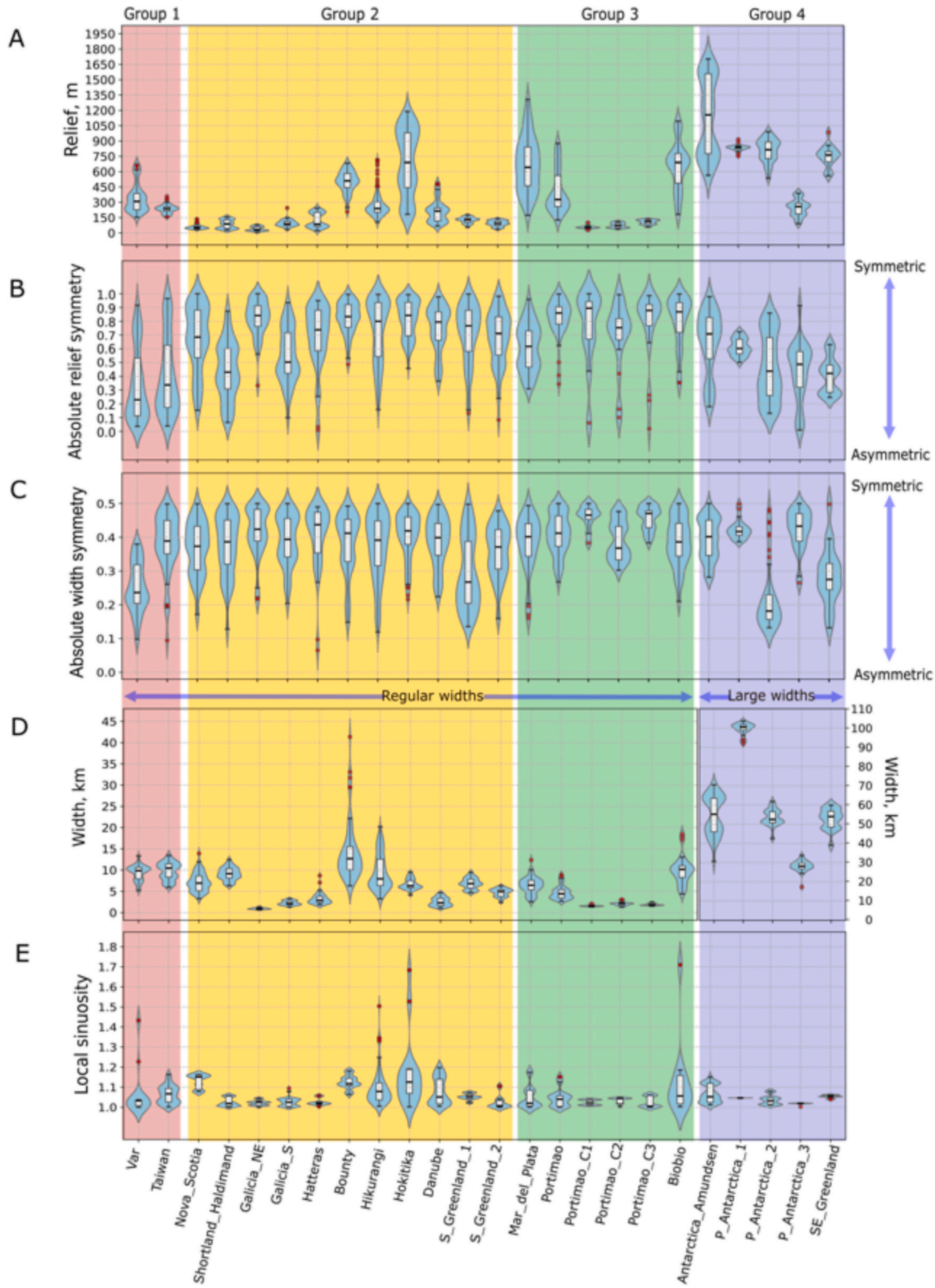

Fig. 5. Statistical distributions of morphological parameters for the 24 measured channels: A) Relief; B) Absolute relief symmetry; C) Absolute width symmetry; D) Width; E) Local sinuosity – all represented as violin plots overlaid with boxplots, with red dots corresponding to outliers. Channels are organized into four groups, which are described in detail in the discussion.

values correspond directly to the mapped segments of each channel.

3. Results

3.1. Overview of study settings

The studied channels are distributed across both the southern and northern hemispheres, with absolute latitudes ranging from approximately 20° to 70° (Fig. 4A). Most channels are situated on passive continental margins, although the Biobio Canyon (Chile) and a channel in northeast New Zealand (Hikurangi) occur on active margins (Fig. 1). Water depths range from less than 500 m to 5 km (Fig. 4B), with the majority of channels located at or below ~2 km water depth on the middle to lower continental slope. The slope angles along the thalweg are generally gentle, with a maximum of 6°, a minimum of nearly 0°, and a median value of 0.33° (Fig. 4C).

3.2. Morphological characteristics of channels

The channels analysed in this study exhibit substantial variability in relief, relief symmetry, width and width symmetry (Fig. 5). Relief ranges from 6 m to 1703 m, with a median of 240 m (Fig. 5A). Width spans from 600 m to 106 km, with a median of approximately 7 km (Fig. 5D). The largest values of both relief and width correspond to broader sedimentary drift-bounded systems rather than the channel alone (Rebesco et al., 1996; Rodrigues et al., 2022a).

Most channels display high absolute relief symmetry, with values exceeding 0.6 (Fig. 5B). However, Var, Taiwan, Antarctica_Amundsen, P_Antarctica_1–3 and SE_Greenland are notably more asymmetric. Var and Taiwan have the lowest median absolute relief symmetry values, at 0.22 and 0.32 respectively. Overall, the variability in both absolute relief symmetry and width symmetry within most channels is substantial, suggesting that no single value of either parameter can adequately characterise a given channel. Fig. 5. Statistical distributions of morphological parameters for the 24 measured channels: A) Relief; B)

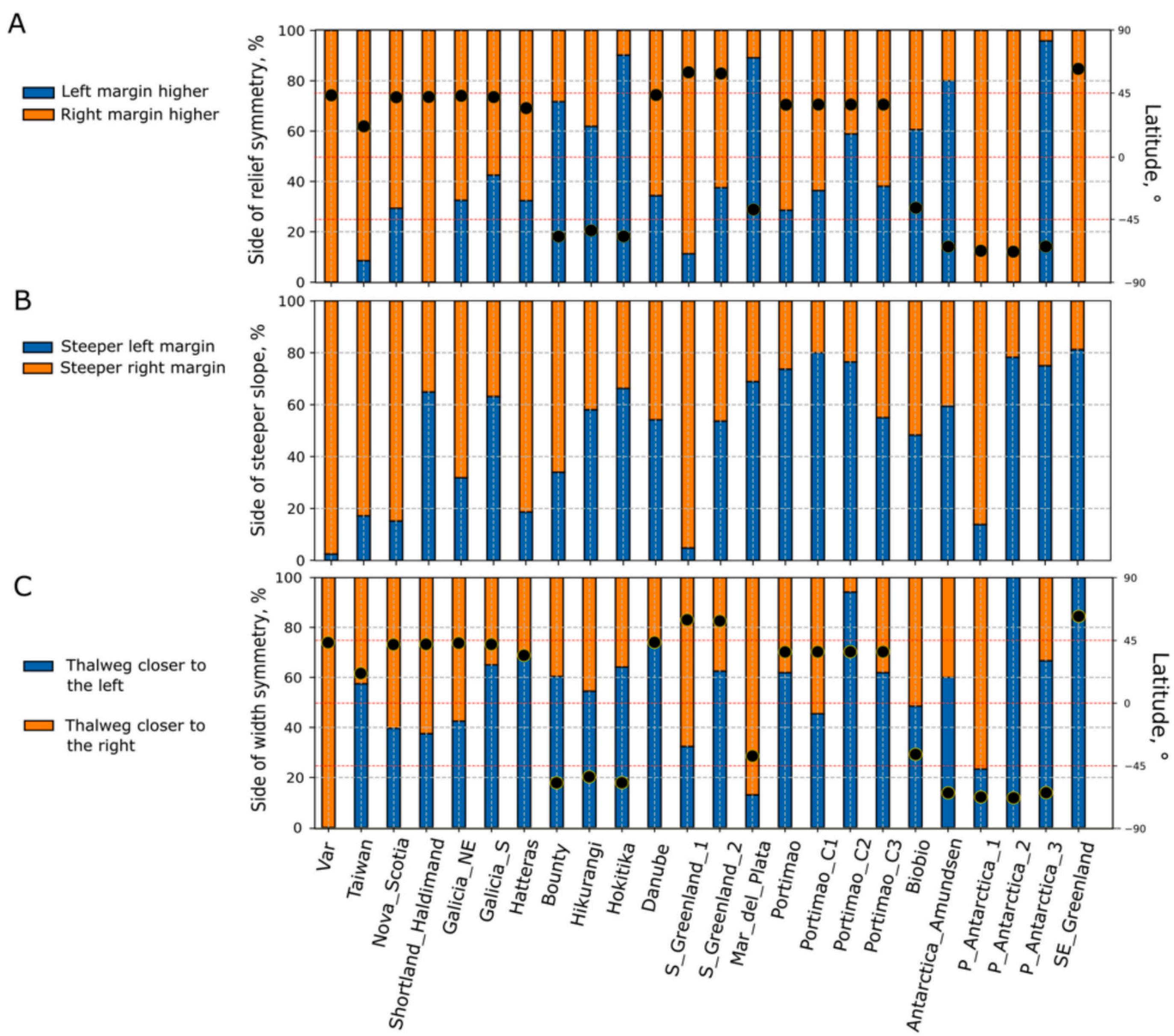

Fig. 6. Stacked bar charts of the 24 measured channels showing: A) Frequency of higher right (orange) and left (blue) margins in percent, with latitude indicated with black dots; B) Frequency of steeper right (orange) and left (blue) margins in percent; C) Frequency of the thalweg closer to the right (orange) and left (blue) margins in percent, with latitude indicated with black dots.

Absolute relief symmetry; C) Absolute width symmetry; D) Width; E) Local sinuosity – all represented as violin plots overlaid with boxplots, with red dots corresponding to outliers. Channels are organized into four groups, which are described in detail in the discussion.

The asymmetric channels analysed here are generally not highly sinuous. Local sinuosity values, calculated for each meander, are typically below 1.21 (Fig. 5E), with a minimum of 1, a maximum of 1.7 and median of 1.05. Measurements of each individual channel are provided in the Supplementary Figs. S1–S29, together with an example of inflection point identification for local sinuosity calculations Fig. S30. The uncertainty in channel width measurements related to bathymetric grid resolution is provided in Supplementary Table S1.

Stacked bar charts reveal that, in most channels, the position of the higher margin varies along the channel, alternating between the left and right sides (Fig. 6A). Similarly, the thalweg varies in position along the channel, lying closer to either left or right margin (Fig. 6C). Only Var, P_Antarctica_1–2 and SE_Greenland maintain a consistent position of a higher margin, and only Var and SE_Greenland maintain a consistent thalweg position (Fig. 6C). In the Var channel, the thalweg is consistently closer to the higher margin, whereas in SE_Greenland, it is closer to the lower margin. In all other cases, the thalweg position relative to the higher margin varies substantially, with width symmetry sides fluctuating more than relief symmetry sides.

Our initial approach measured only width symmetry, under the hypothesis that the thalweg would always be positioned closer to the steepest margin, making width symmetry a suitable proxy for cross-sectional slope angles. However, manual measurements of cross-sectional slope angles show that this assumption does not always hold: in at least six channels, the steeper margin is most often opposite the side nearest to the thalweg (Fig. 6B).

The position of the higher margin generally aligns with the expected Coriolis pattern – on the right side in the northern hemisphere and on the left side in the southern hemisphere. Exceptions include the two channels on the Pacific margin of Antarctica (P_Antarctica_1–2), where the higher margin is on the right despite their southern hemisphere location, and Portimão_C2, where ~60% of cross-sections show a higher left margin. In contrast, the positions of the steeper margin and the thalweg show no clear relationship with latitude (Fig. 6B–C).

Relief does not display a direct correlation with symmetry values, but it appears to act as a threshold: channels with greater relief are less likely to exhibit low-symmetry cross-sections (Fig. 7A, B). This threshold effect is more evident for relief symmetry than for width symmetry, suggesting that thalweg position is less sensitive to relief variations. Absolute relief symmetry is independent of latitude (Fig. 7C).

A weak positive linear correlation is observed between cross-sectional slope angle and relief ($R^2 = 0.46$, Fig. 7D). This suggests that slope angle, like relief, may act as a threshold influencing symmetry, but the effect appears even weaker than for relief, with a large amount of variance not explained by these variables in isolation.

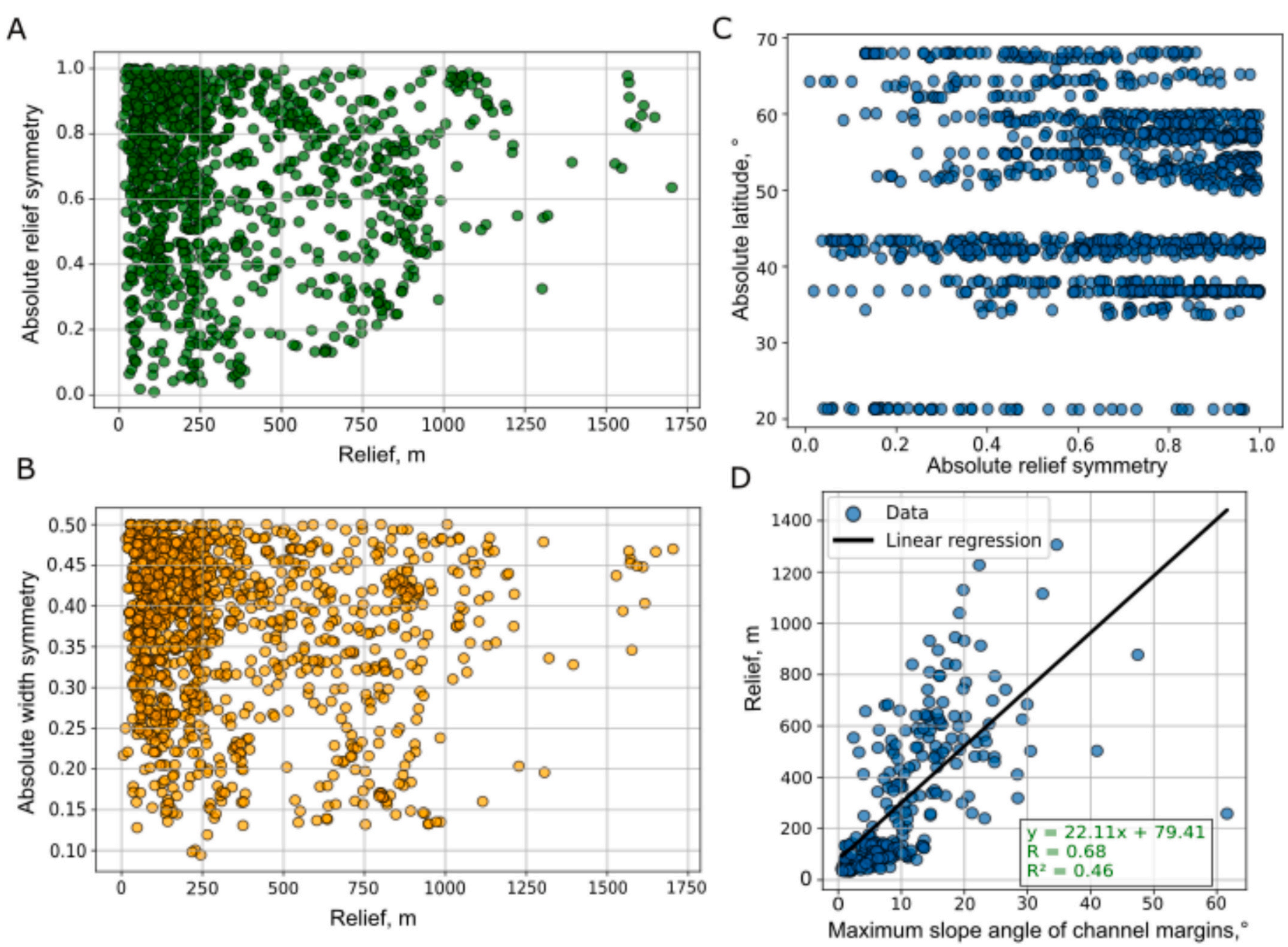

Fig. 7. Relationships between channel morphological parameters for the 24 measured channels: A) Relief versus absolute relief symmetry; B) Relief versus absolute width symmetry; C) Absolute relief symmetry versus absolute latitude; D) Maximum slope angle of channel margins versus relief with linear regression indicated.

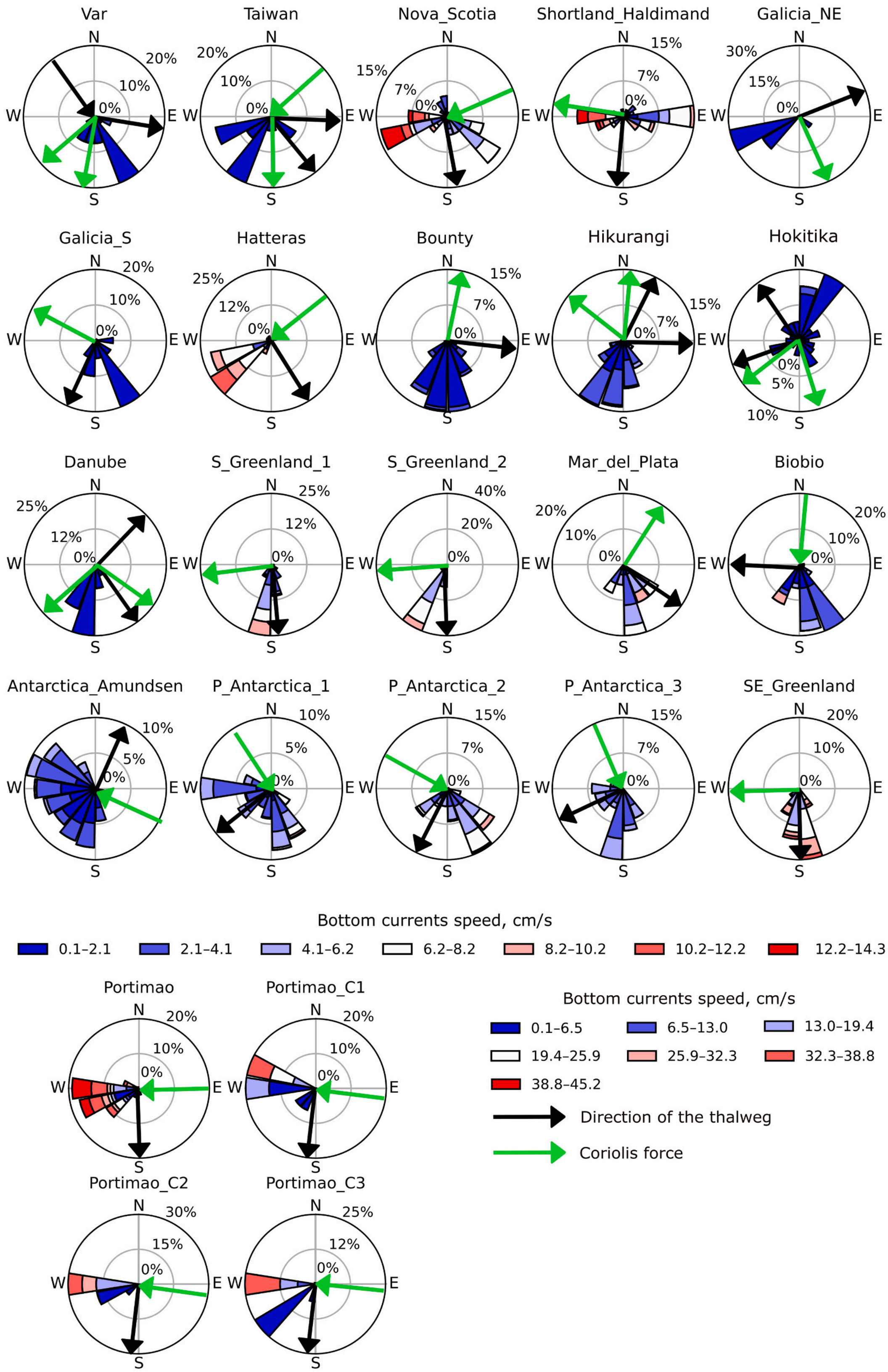

Fig. 8. Rose diagrams of bottom current direction and speed for the measured channels, thalweg direction and the effect of the Coriolis force on turbidity currents direction are indicated. Note that the colour scale for bottom currents at the Portimão canyon is different.

3.3. Bottom currents at the channel sites

The magnitude of bottom current velocities extracted at each channel vary from 0.1 cm/s to 45 cm/s at Portimão and neighbouring Portimão_C1–C3 channels. At the majority of channels bottom currents do not reach magnitudes above 10.2 cm/s (Fig. 8).

The angle between the thalweg direction and the most frequently observed flow direction varies spatially and is not uniform (Fig. 8). While in some locations such as Shortland_Haldimand, Hatteras, Antarctica_Amundsend and Portimão, the angle is nearly 90°, in others it is significantly smaller or larger. In several locations segments of bottom currents are directed along the thalweg, and in the southeastern Greenland (SE_Greenland) and Var system, the predominant flow direction coincides with the orientation of the thalweg. In Var, Taiwan, Hikurangi, Hokitika and Danube channels the thalweg undergoes significant directional changes, which may alter the interaction between bottom currents and turbidity flows along these channels.

3.4. Channel groups

The high variability of morphological parameters, combined with the absence of clear correlations among them, highlights the complexity of the processes shaping asymmetric channels and suggests that there is no common trend for all systems. Nevertheless, by integrating both environmental and morphological data, we applied a hybrid geomorphological classification approach combining quantitative metrics and diagnostic morphological characteristics, and identified four distinct groups: Group 1 – Channels with extreme asymmetry (median absolute relief and width symmetries <0.4); Group 2 – Channels with clear levees and possible sediment waves, encompassing a range of channel types, including isolated deep-ocean systems, showing low to medium asymmetry (median absolute relief symmetry 0.4–0.85, width symmetry

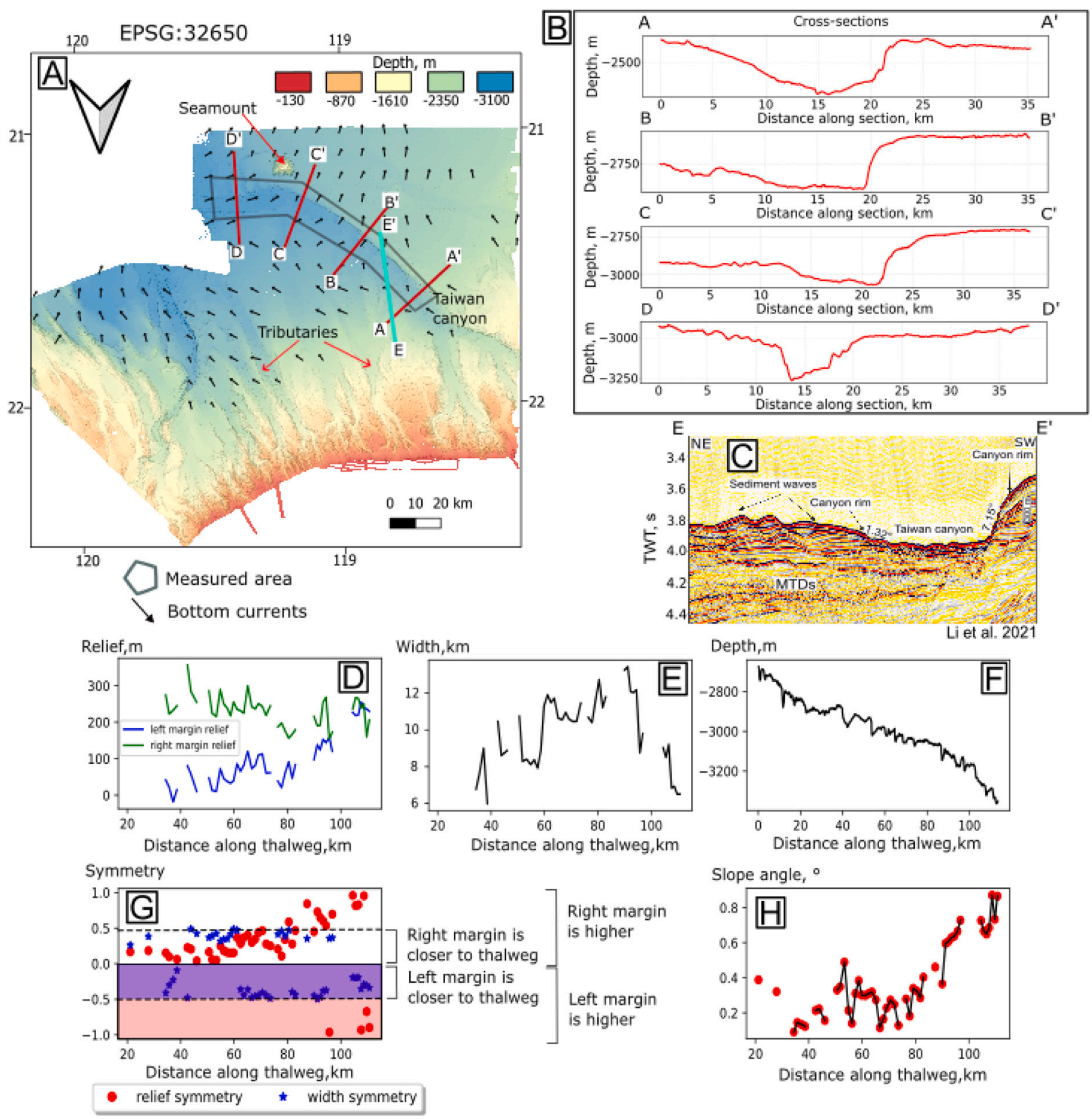

Fig. 9. Morphological characteristics, seismic profile, and bathymetry map overlaid with bottom currents at Taiwan system: A) Bathymetry map; B) Depth profiles at cross-sections specified in the bathymetry map; C) Seismic profile modified from Li et al. (2021), the position is specified on the bathymetric map; D) Relief along the measured thalweg; E) Width along the measured thalweg; F) Depth along the measured thalweg; G) Relief and width symmetries along the measured thalweg; H) Slope angle along the measured thalweg.

>0.3); Group 3 – Channels without clear levees, predominantly canyons, sometimes coexisting with contourite depositional systems, with low to medium asymmetry (median absolute relief and width symmetries 0.6–0.9 and 0.35–0.48, respectively); Group 4 – Large submarine systems at high latitudes, characterised by broad valleys with smaller internal channels between asymmetric sedimentary drifts (median absolute relief and width symmetries 0.4–0.7 and 0.18–0.45, respectively).

However, each group encompasses a considerable internal variability, reflecting the fact that some channels evolve along a continuum from canyon-like to fully developed channel-levee systems, and may also be influenced by varying degrees of interaction with bottom currents and other modifying processes. As a result, the group boundaries should be understood as conceptual rather than strictly discrete. Representative examples of channels for each group are shown below, while the rationale and interpretation of this classification are provided in the Discussion. A summary of the classification of submarine channels and canyons and their main characteristics is given in Supplementary Table S2.

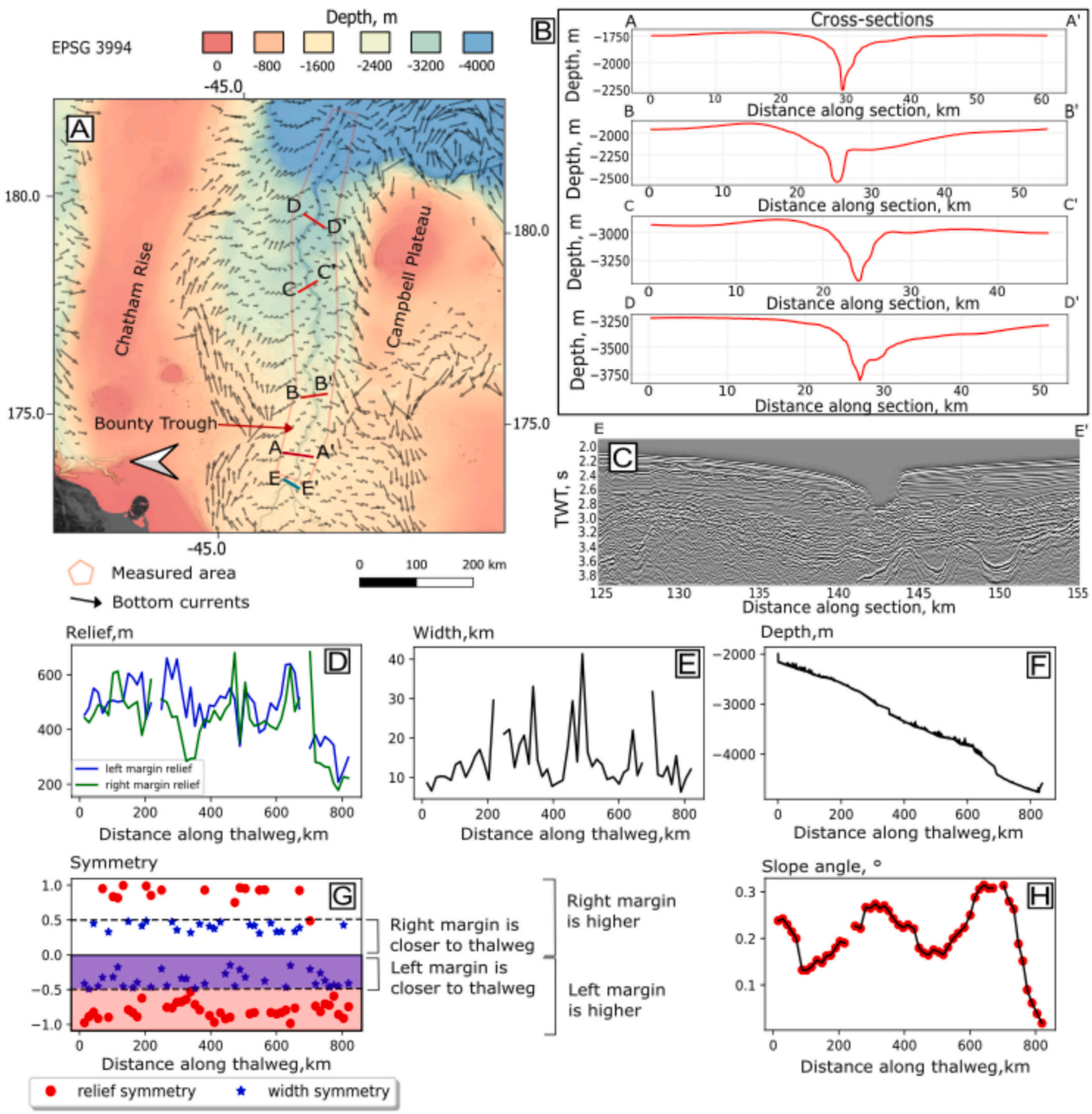

Fig. 10. Morphological characteristics, seismic profile, and bathymetry map overlaid with bottom currents at Bounty channel: A) Bathymetry map; B) Depth profiles at cross-sections specified in the bathymetry map; C) Seismic profile (Line BT10-02M1000) obtained from the 2018 New Zealand Petroleum Exploration Data Pack, the position is specified on the bathymetric map; D) Relief along the measured thalweg; E) Width along the measured thalweg; F) Depth along the measured thalweg; G) Relief and width symmetries along the measured thalweg; H) Slope angle along the measured thalweg.

3.4.1. Group 1 - Taiwan system

The Taiwan system is located in the north-eastern part of the South China Sea (Fig. 1). The system is measured at a water depth ranging from 2800 to 3300 m. The measured length is approximately 113 km long and 6 to 12 km wide (Fig. 9A; Li et al., 2021). Our measurements cover most of the middle reach of the system between 2500 m and 3125 m (Li et al., 2021). The beginning of the lower reach is between 3125 m and 3500 m according to Li et al. (2021). The margins of the middle reach are

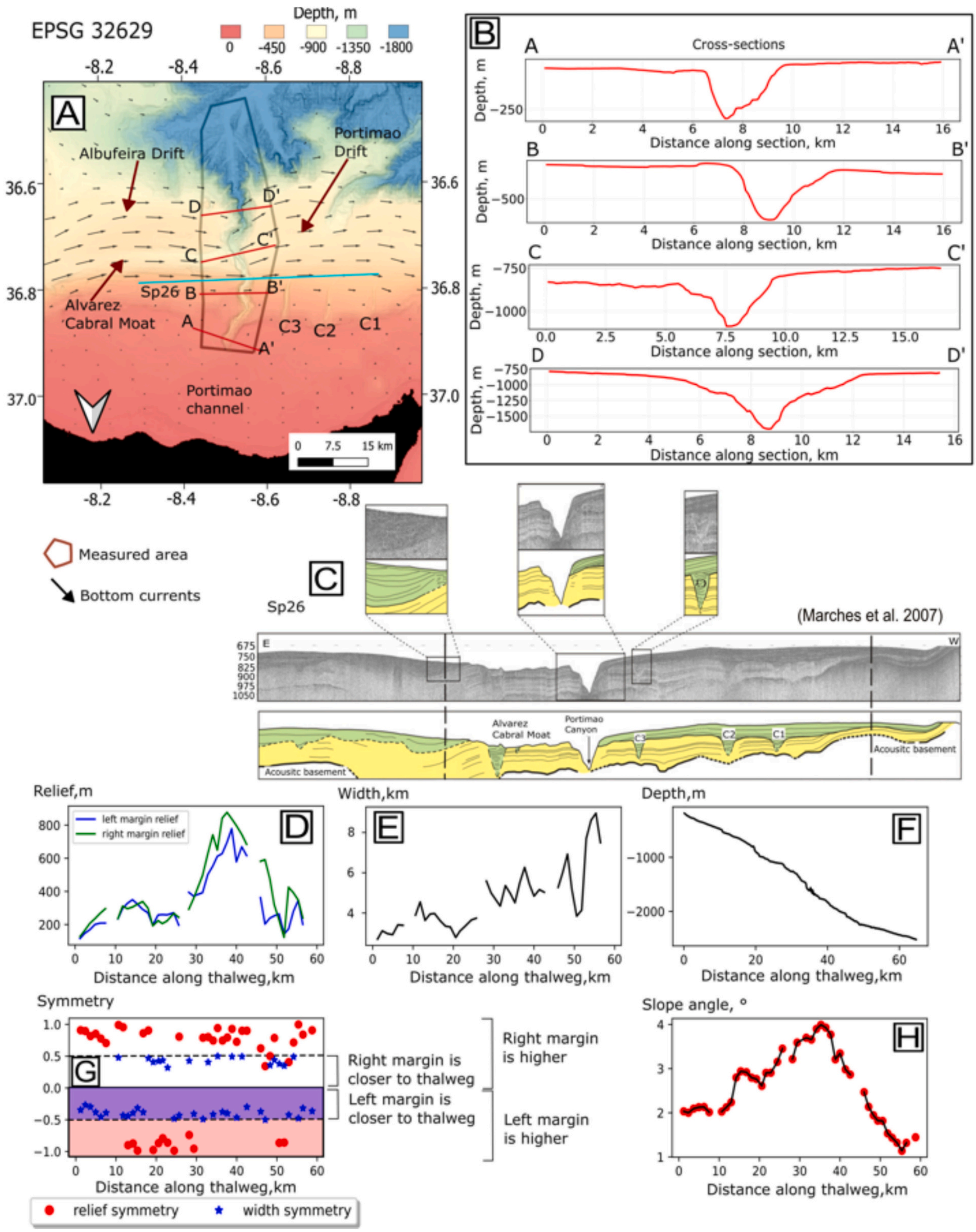

Fig. 11. Morphological characteristics, seismic profile, and bathymetry map overlaid with bottom currents at Portimão canyon: A) Bathymetry map; B) Depth profiles at cross-sections specified in the bathymetry map; C) Seismic profile modified from Marchès et al. (2007), the position is specified on the bathymetric map; D) Relief along the measured thalweg; E) Width along the measured thalweg; F) Depth along the measured thalweg; G) Relief and width symmetries along the measured thalweg; H) Slope angle along the measured thalweg.

asymmetrical in both their height and slope angle (Li et al., 2021) (Fig. 9B sections AA′, BB′, CC′). The relief of the right south-west margin is around 300 m while the relief of the left north-east margin is mostly below 150 m (Fig. 9D).

Li et al. (2021) further reported the presence of levees with sediment waves within the southern flank of the lower part of the system (Fig. 9C), which they interpreted as evidence for overspill, indicating that the Taiwan system is not purely erosive.

The orientation of the canyon changes from south-east to nearly east-west with the transition from the middle to low reach of the canyon at about 100 km along the measured thalweg. The transition to the lower reach is coincident with a faster increase in slope angle, an increase in relief symmetry to above 0.8, and decrease in the width from 10 km to 8 km (Fig. 9E). The left margin in the lower reach is comparable or higher than its counterpart (Fig. 9D). The position of the thalweg is nearly central with overall slight deviation to the left margin, except parts between 40 and 60 km, 80 and 95 km along the measured thalweg, where it is slightly deviated to the right (Fig. 9G). The shape of the canyon changes downstream from U-shape (AA′) to flat trapezoid (BB′, CC′) and trapezoid in the lower reach (DD′) (Fig. 9B).

In the north-eastern part, mass transport deposits are identified on seismic profiles, appearing as discontinuous transparent reflections (Li et al., 2021) (Fig. 9). Li et al. (2021) suggested that the controlling factor of relief asymmetry is the erosion by recurrent slope failures to the north-east of the Taiwan canyon. Moreover, the tributaries to the north-east of the Taiwan canyon (Fig. 9A) could be a factor that results in increased erosion of the left north-east margin in present time.

3.4.2. *Group 2 - Bounty channel*

The Bounty channel is located in the Bounty Trough to the south-east of Aotearoa New Zealand. The measured part of the channel is nearly 837 km long from 2196 to 7740 water depth (Fig. 10A, E). The channel is deep with a relief often above 400 m and a width commonly between 10 and 20 km. The relief symmetry is relatively high exceeding 0.5, and the side of the higher margin frequently changes, however the left margin is more often higher than the right. The same applies to the width symmetry, the thalweg is preferably deviated to the left. The slope angle along the measured thalweg is within the range from nearly 0° to 0.3°.

The channel has a more defined left levee and maintains a consistent V-shaped cross-sectional profile along its length. The left margin is steeper than the right one (Fig. 10B). Predominantly higher left margin of the Bounty channel aligns with the expected influence of the Coriolis force. The frequent fluctuations of the position of the higher margin could be explained by centrifugal force and bottom currents, which Carter and Carter (1988) hypothesized to flow northeastward. However, in this case we do not observe a correlation between the local sinuosity, the orientation of the meander and the relief symmetry (Fig. 10B, section CC′ and DD′). These sections are located on two opposite sides of a meander, and in both cases the left margin is higher. Besides, ocean reanalysis data suggests that bottom currents in the area mainly flow southward along slope and therefore are unlikely to contribute to the growth of the left levee (Figs. 8 and 10). Although the channel is deep (relief ranging between 200 m and 400 m), the levees are well-defined with presence of sediment waves (Carter and Carter, 1996), that indicates overspilling.

3.4.3. *Group 3 – Portimão canyon*

The Portimão canyon is situated in the Gulf of Cádiz, north-western Atlantic Ocean (Fig. 1). The measured length is about 65 km at water depth between 240 and 2410 m (Fig. 11). The relief oscillates from around 200 m at the head of canyon to about 800 m at 30 km along the thalweg where the canyon separates Albufeira and Portimão drifts. The width is not very high, increasing from 4 km to up to 8 km at the place where Portimão flows into a bigger canyon system (Fig. 11A). The slope angle is relatively high. In the first 50 km along the measured thalweg, it is within the range from 2° to 4°. Further down the slope angle sharply decreases to 1°. The relief increases with increasing slope angle and vice versa (Fig. 11D, H).

The relief asymmetry is generally low (absolute symmetry values are around 0.8), the right margin is usually higher except for a small area before Álvarez Cabral Moat (Fig. 11B, section BB′) and an even smaller area located at the lower part of Albufeira drift at about 50 km along the measured thalweg. Between 30 and 40 km the presence of the moat increases the difference in relief between left and right margins, enhancing the asymmetry. The channel maintains V-shape cross-section along the entire measured thalweg. We observe erosional features on seismic data on one or both flanks (Fig. 11C; Marchès et al. (2007)).

The Portimão canyon coexists laterally with contourites – Álvarez Cabral Moat, Albufeira and Portimão Drifts (Fig. 11A). These contourites affect the canyon relief symmetry as well as the presence of canyon affects the morphology and sedimentation processes of these contourites (Marchès et al., 2007). We observe an enhanced erosion on the left margin when Alvarez Cabral Moat meets Portimão canyon (Fig. 11B, section CC′).

3.4.4. *Group 4 - Pacific margin of Antarctica*

The channel described in this section is referred to as P_Antarctica_2 in Figs. 4–6. For the channels along the Pacific margin of the Antarctic Peninsula, we considered margins as features which Rebesco et al. (1996) and Rodrigues et al. (2022a) described as sediment drifts formed by the deposition of material transported by turbidity currents that is picked up by contour currents. It should be noted, however, that these drift-related margins are not part of the channel itself, but rather belong to a broader system in which a smaller internal channel is embedded. Although such systems do not correspond strictly to channels, they have been widely interpreted as mixed turbidite-contourite systems and are therefore included as examples of large-scale interaction between bottom currents and turbidity currents (Rebesco et al., 1996; Rodrigues et al., 2022a). Widths measured between margins are above 40 km (Fig. 12E), the margins demonstrate high relief (Fig. 12D) and width asymmetries, and consistency of the asymmetries' sides (Fig. 12G). The thalweg is always closer to the lower and steeper left margin, which is mostly 500 m lower than the right.

The slope angle is relatively low, ranging between 0.1° and 0.5° (Fig. 12H). Two depressions with subsequent elevations within the first 40 km are observed along the measured thalweg (Fig. 12F). The two depressions along the thalweg correlate with the increase in width (Fig. 12E). In this case, the higher right margin develops opposite to the direction expected from the Coriolis effect. The right margin of the described channel also serves as the left margin of the adjacent P_Antarctica_1 (Fig. 12A, C).

4. Discussion

By analysing a globally distributed dataset, extracting bottom-currents from models precisely at locations of studied channels, and applying a flexible morphometric analysis tool, this study demonstrates that channels exhibit substantial variability in their cross-sectional geometry – often even within the same system. This variability reflects the fact that environmental and hydraulic conditions change markedly with depth, including variations in slope gradient, water-mass properties, turbidity-current density and momentum, bottom-current intensity and direction, and channel dimensions. Consequently, the relative influence of Coriolis forcing, buoyancy effects, flow momentum, and contour-current shear also shifts along a channel's course. While these factors may produce locally coherent and interpretable patterns of asymmetry, they cannot be used to reliably predict channel characteristics at different depths within the same system. This highlights the need for caution for inferring controlling processes solely from channel morphology or sedimentary architecture.

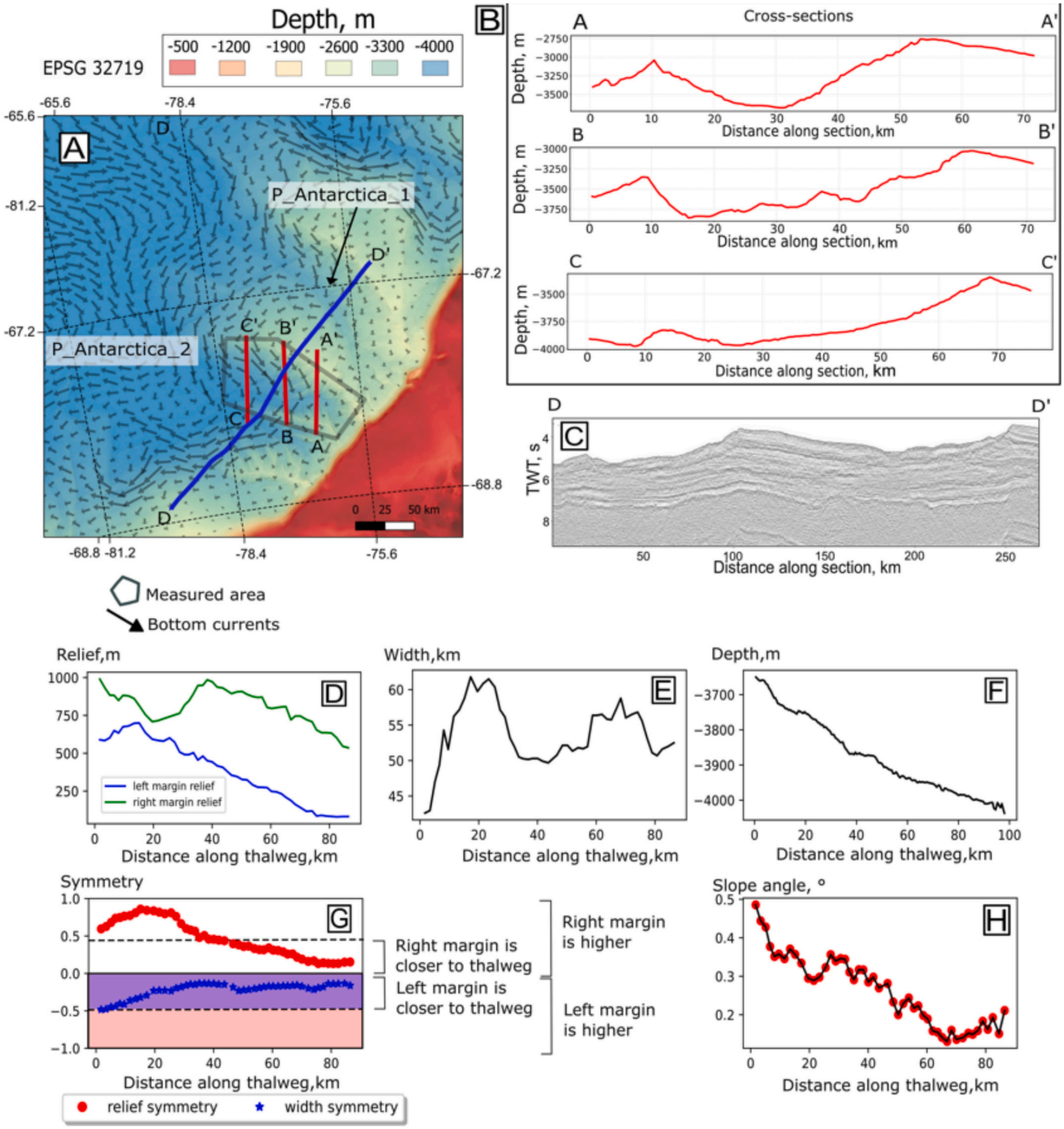

Fig. 12. Morphological characteristics, seismic profile, and bathymetry map overlaid with bottom currents at Pacific margin of Antarctica P_Antarctica_2 channel: A) Bathymetry map; B) Depth profiles at cross-sections specified in the bathymetry map; C) Seismic profile (EW91010-1079) from the Antarctic Seismic Data Library System for Cooperative Research accessed through the GeoMapApp, the position is specified on the bathymetry map; D) Relief along the measured thalweg; E) Width along the measured thalweg; F) Depth along the measured thalweg; G) Relief and width symmetries along the measured thalweg; H) Slope angle along the measured thalweg.

4.1. Classification of asymmetric channels

We classify channels based on their morphological and environmental characteristics to identify recurring patterns and provide a framework for interpreting the processes contributing to channel asymmetry (Fig. 13). Previous studies have proposed models of interactions between turbidity currents and bottom currents, including synchronous, passive, and phased interaction models (Fonnesu et al., 2020; Mulder et al., 2008). We reference these interaction types here, because they provide a useful framework for interpreting our own classification. Importantly, our classification is channel-based, and is applied at the scale of entire channels rather than individual segments. As a result, different parts of a single channel may correspond to different classes, although we do not subdivide channels in this way.

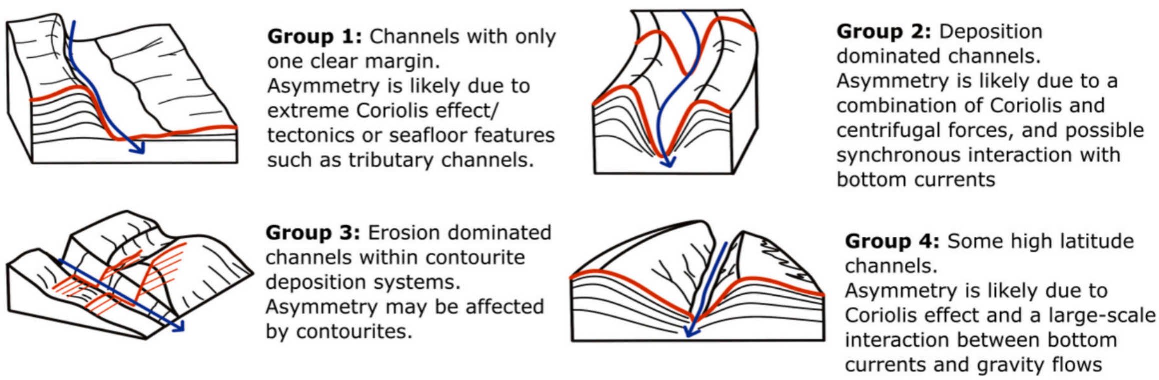

Fig. 13. Schematic summary of the classification of asymmetric channels.

Group 1 – Channels with extreme asymmetry (median absolute relief symmetry values below 0.4, Fig. 5B), such as Taiwan and Var systems, where the asymmetry is mainly caused by extreme Coriolis effect or tectonics, or seafloor features such as tributary channels or seamounts.

Group 2 – Channels with clear levees and possibly sediment waves, demonstrating low to medium asymmetry (median absolute relief symmetry values above 0.4, Fig. 5B), possibly asymmetric due to Coriolis effect and centrifugal forces. These channels also have the potential for synchronous interaction with bottom currents, which should be validated using direct measurements or flow modelling.

Group 3 – Channels without clear levees, coexisting with a contourite depositional system and sometimes affected by mass-wasting processes. The absence of well-developed levees may reflect the predominantly erosional character of these systems, supporting their interpretation as canyons. Here, asymmetry appears to be indirectly controlled by passive interaction with bottom currents (e.g., Portimão canyon). Channels in this group generally occur along steeper slopes, at shallower depth than other groups (Fig. 4B, C), exhibit relatively uniform width symmetry, and low to medium relief asymmetry (Fig. 5B).

Group 4 – Channels at high latitudes (Fig. 5D), such as channels in the Pacific margin of Antarctica and southeast Greenland, located between asymmetric sedimentary mounds oriented downslope. The asymmetry of these mounds may reflect the Coriolis effect and large-scale interaction with bottom currents.

4.2. *Factors contributing to channel asymmetry*

4.2.1. *Coriolis force*

Coriolis force has been considered one of the key factors explaining relief asymmetry in constructional submarine channels (Cossu et al., 2015, 2010; Wells and Cossu, 2013). Coriolis force primarily has a strong influence on gravity flows at higher latitudes, where the Rossby number (i.e., the ratio between the inertial force and the Coriolis force) is low. This may result in a deflection of the core of gravity flows within channels, toward the left in the southern hemisphere and toward the right in the northern hemisphere, forming higher left levees in the southern hemisphere and higher right levees in the northern hemisphere, when the flow is relatively weak and dominated by suspension fallout (Cossu et al., 2015). In contrast, when flows are highly energetic and dominated by traction, deposition may occur on the opposite side of the core of the turbidity current and levees tend to be smaller (Cossu et al., 2015).

In this study, the position of the higher channel margin varies along the length of most channels. Nevertheless, the majority of cross-sections demonstrate the position of a higher margin consistent with the direction of the Coriolis force (Fig. 6). Two notable exceptions are found along the Pacific margin of Antarctica, where the higher margin is located on the right side, contrary to the expected pattern for the Southern Hemisphere (Fig. 12G). We suggest that the presence of adjacent channels resulting in two channels sharing one margin may be responsible for this deviation (Fig. 12C).

The position of the thalweg relative to the centre of a cross-section also varies along the length of individual channels and within the same hemisphere, suggesting that it is not primarily controlled by the Coriolis force (Fig. 6). Furthermore, the weak global correlation between local sinuosity and width symmetry (Fig. 5) indicates that, for the mostly low-sinuosity channels in our study, centrifugal forces associated with channel curvature do not solely determine thalweg position. Instead, thalweg position likely reflects a complex and spatially variable interaction between these forces, seafloor morphology, and bottom current activity. Consequently, isolating the individual influence of each factor along the channel's course is not feasible.

Channels at high latitudes can exhibit relatively low asymmetry – for example, the south Greenland channel (S_Greenland_1) shows an absolute relief symmetry value of approximately 0.8 – while some mid-latitude channels, such as the Var and Taiwan systems, display much higher asymmetry, with values around 0.4 (Fig. 5). This observation suggests that Coriolis force does not solely control the degree of channel asymmetry. Instead, the degree of asymmetry may be influenced by a combination of factors, including seafloor morphology, channel confinement, mass-wasting processes (e.g., slumps or slides).

4.2.2. *Centrifugal force*

Centrifugal forces act on turbidity currents flowing through channel bends, driving the flow toward the outer bank, promoting erosion and levee development on that side, which in turn increases channel sinuosity (Dorrell et al., 2013; Imran et al., 1999; Sylvester and Pirmez, 2019). These forces dominate when the Rossby number is high, reflecting a reduced influence of the Coriolis force.

The channels analysed in this study have generally low sinuosity, with local sinuosity values ranging between 1 and 1.3 (Fig. 5E). Following standard classifications for fluvial and submarine channels (e.g., Wynn et al., 2007), values below 1.2 are typically considered straight, indicating that most systems in this dataset fall within straight category despite minor variations in planform curvature. This contrasts with highly sinuous systems such as the Congo, Amazon, and Nile, where sinuosity can exceed 3 (Sylvester and Pirmez, 2019). Low sinuosity with limited variability may partly explain the weak correspondence between channel asymmetry and local sinuosity (Fig. 5A, B and E), as well as the potentially minor influence of centrifugal forces.

According to Peakall et al. (2012), the Coriolis force may influence the global distribution of submarine channel sinuosity, which could contribute to lower sinuosity in high-latitude channels. However, this relationship is likely multifactorial, with additional controls including flow dynamics and sediment supply, as clarified in Peakall et al. (2013). Examples illustrating such variability include the Danube channel (43°–44°N; Sylvester and Pirmez (2019)), as well as the Danube Fan and Knight Inlet (approximately 44°N and 51°N; Sylvester et al. (2013)), which exhibit relatively high sinuosity and pronounced relief asymmetry. These observations fall within or near cut-off for high-sinuosity systems (about 50°N latitude) suggested by Peakall et al. (2013), and, as noted by Allen et al. (2022), no comparable highly sinuous channels are known outside this range. These examples suggest that Coriolis-induced asymmetry can coexist with subtle or low-amplitude meandering, as observed in the Bounty channel (Fig. 10A). This could be explained by vertical stratification of turbidity flow: the lower, faster and coarser-grained layer may be governed primarily by centrifugal forces, promoting meandering, while the upper, slower and finer-grained layer may be more affected by the Coriolis effect (Cossu et al., 2015). This may also account for the observed displacement of the thalweg toward the lower margin in some channels (Fig. 6).

4.2.3. *Channel confinement*

In confined channels lacking well-developed levees, which are indicative of limited or absent overspill, the influence of the Coriolis and centrifugal forces, as well as synchronous interaction with bottom currents on channel asymmetry is likely minimal. In such cases, other processes, such as slope instability, internal flow dynamics and passive interaction with bottom currents, may play a more dominant role in shaping channel morphology. While the degree of confinement is commonly expressed as the ratio of flow thickness to channel depth (h/D; Adema et al., 2025b; Mohrig and Buttles, 2007), we do not have direct flow thickness data. Nevertheless, our observations suggest that relief can serve as a first-order proxy for confinement: channels with higher relief tend to exhibit fewer cross-sections with pronounced asymmetry (Fig. 7A, B), whereas channels with lower relief may display more varied asymmetries.

The character of the turbidity flow – whether depositional or traction-dominated – is also an important factor. Depositional flows are more likely to result in the formation of levees, whereas traction-dominated flows typically do not, regardless of channel relief (Cossu et al., 2015).

4.2.4. *Bottom currents*

Bottom currents - particularly contour currents - have been demonstrated to be capable of deflecting turbidity currents (Fuhrmann et al., 2020; Hernández-Molina et al., 2022; Miramontes et al., 2020; Rodrigues et al., 2022a,b; Adema et al., 2025a, 2025b), and also modifying sedimentary systems and forming contourite depositional features such as contourite terraces, moats and contourite drifts (Miramontes et al., 2019, 2021; Rebesco et al., 2014; Wilckens et al., 2021). These currents are primarily steered by the Coriolis force, which could complicate the attribution of channel asymmetry to their influence, especially because the Coriolis force acting on turbidity currents and contour currents tend to act in the same direction (Fig. 8).

The potential for synchronous interaction critically depends on the interplay between turbidity-current and bottom-current properties – particularly the velocity of both flows and the density structure of the turbidity current (Miramontes et al., 2020). Understanding this interaction is challenging, however, because of the lack of direct observations and measurements of both turbidity currents and near-bed contour currents at field scale. This means that we have had to rely upon scaled-down experimental models and numerical models to inform our interpretation of depositional geometries.

Some conceptual and experimental studies have suggested that interactions between turbidity currents and contour currents may primarily affect the upper, more dilute portion of the flow, while the basal, higher-concentration core remains less influenced (Fonnesu et al., 2020; Miramontes et al., 2020; Rodrigues et al., 2022b). However, more recent works indicate that this interaction can be more complex and may involve the full depth of the turbidity current. For example, Adema et al. (2025a, 2025b) and Zhang et al. (2026) demonstrated that contour currents can influence not only the upper flow but also basal layers and associated sediment transport. These findings suggest that the extent of interaction likely depends on flow structure, sediment concentration, and ambient current conditions. Field observations of turbidity currents in settings affected by contour currents from the Var system indicate that while the core of the turbidity current in the thalweg is fast-moving, the upper part of the flow is much slower (of the order 20 cm/s), which is comparable to the ambient contour current velocity (2–10 cm/s) (Khripounoff et al., 2012). Therefore, interaction may be more likely to affect the upper part of the flow in this setting, and may not substantially deflect the flow laterally because both turbidity currents and bottom currents share the same down-canyon orientation. Consequently, asymmetric sediment accumulation in that setting is thought to be more strongly controlled by the influence of Coriolis force (Payo Payo, 2016). Therefore, even in settings where there is a synchronous interaction, we do not necessarily expect there to be a major control on channel asymmetry.

The Bounty channel was suggested to be affected by bottom currents (Carter and Carter, 1988). While regional currents (Southland current, western boundary current) generally flow northward (Carter and Carter, 1988), near-bottom currents with a maximum speed of 4 cm/s right above Bounty channel tend to move southward (Figs. 8 and 10A). This may result from the trapping of northward flow between the Chatham Rise and Campbell Plateau (Fig. 10A), where interactions with regional bathymetry promote the formation of a gyre that reverses current direction; hence, the asymmetry of the Bounty channel is more likely mainly influenced by Coriolis force.

The near-bottom current model data used in this study spans a long time period (28 years for most locations) and should therefore be interpreted with caution, particularly because modelled currents typically underrepresent episodic velocity peaks observed in situ. While monthly mean velocities provide a useful indication of prevailing bottom-current conditions, key interactions likely depend on factors such as directional persistence, episodic intensification, and timing relative to turbidity currents. The model results suggest that mean bottom current velocities at the studied channels are generally low – typically below 10 cm/s – except in regions such as the Portimão and adjacent C1-C3 channels, where velocities reach up to 45 cm/s and significant contourite features are observed (Fig. 8). The channel margins of the Portimão system (Fig. 11) is significantly influenced by the presence of contourites, leading to enhanced asymmetry and shift in the position of the higher margin. This may represent an example of passive interaction, where bottom currents modify channel morphology indirectly through differential sediment accumulation within the drift and the moat (Fig. 11). Variability along individual channels and differences in model resolution could contribute to uncertainty in interpreting bottom-current influences.

Seafloor topography can strongly deflect bottom currents. Therefore, the initial channel morphologies created by gravity flows can then affect bottom-current dynamics and often induce bottom currents flowing parallel to the channel margins (Bailey et al., 2024; Miramontes et al., 2019). Bottom currents may become steered along the axes of submarine channels, as observed on the Pacific margin of Antarctica and southeast Greenland (Figs. 8 and 12). In these regions, the channel relief can exceed 1 km, and the channel margins are widely spaced, suggesting that bottom currents may become confined or guided by the channel morphology. Rebesco et al. (1996) suggested that contour currents played a significant role in forming margins of channels in the Pacific margin of the Antarctic Peninsula. Large amounts of sediment coming during glacial periods were suggested to be deposited on the flat margin by south-westerly contour currents, while the right margin was subjected to slope instabilities (gullies) (Fig. 12C). Rebesco et al. (1996) emphasized that the large relief of the mounded features could not be explained by the Coriolis effect alone, pointing instead to bottom current involvement. More recent work by Rodrigues et al. (2022b) supports this interpretation and shows that mixed turbidite-contourite systems in the region record phases of synchronous interaction, particularly during glacial intervals when sediment supply was highest. These periods of interaction were followed by phases dominated by intensified bottom current activity, which reworked and stratified the deposits.

These results highlight the need to reassess assumptions about bottom current directions when evaluating their interactions with turbidity flows. Seafloor morphology can significantly alter current pathways, and bottom currents right above a channel may not necessarily follow the same direction as those near the channel.

We hypothesized that in the case of synchronous interaction, the steeper channel margin would be situated upstream of the bottom current direction. However, our observations (Figs. 6 and 8) show no consistent pattern: in some channels the steeper margin is more frequently located downstream of the bottom current direction, whereas in others the opposite is true. Moreover, the position of the steeper margin often shifts along the length of individual channels. This lack of systematic alignment suggests that bottom currents are unlikely to be the primary control on the development of a steeper channel margin. This observation is consistent with recent flume tank experiments (Adema et al., 2025b), which show that once a steeper margin has developed, the velocity maximum of the turbidity current tends to lean toward that side, with or without the presence of bottom currents. Such flow steering may further enhance the steepness of the established margin.

5. Conclusion

In this study, we analysed the morphological characteristics and environmental context of 24 asymmetric channels from diverse global locations to identify key factors influencing their asymmetry. A Python-based tool was developed to consistently extract morphological parameters. Our results reveal substantial variability in relief and width symmetries, as well as in channel width, relief and slope angle along thalweg. Both the degree of asymmetry and the positions of the higher margin, steeper margin and thalweg vary along channel lengths.

Coriolis forces emerge as a primary control on the location of the higher margin, although local seafloor features occasionally disrupt this pattern. Notably, the position of the steeper margin does not consistently correspond to the thalweg location, indicating that distinct processes may govern channel incision versus margin formation.

The generally low sinuosity of channels suggests minimal **centrifugal force** influence; however, when aligned with Coriolis direction, centrifugal forces may enhance asymmetry. Vertical stratification in turbidity flows could enable centrifugal forces to affect the dense lower layer, while Coriolis forces dominate the lighter upper layer, potentially explaining instances where the thalweg lies nearer the lower margin.

Bottom current data from the ocean reanalysis highlight the strong influence of seabed topography on current pathways, which in some cases results in bottom current directions that differ from previous assumptions – for example in the Bounty channel. In some other settings, such as the Var system, bottom currents predominantly flow along the channel axis rather than across it, indicating that their contribution to channel asymmetry is likely minimal.

Channel confinement strongly influences the expression of asymmetry. In confined channels lacking well-developed levees, the effects of Coriolis force and synchronous interaction with bottom currents are likely minimal, with slope instabilities, internal flow dynamics, and passive bottom current interaction playing a larger role. Higher-relief channels generally show fewer cross-sections with pronounced asymmetry, reflecting limited overspill.

Seafloor morphology, related to gullies, slumps, tributaries and contourites influence asymmetry in the Var and Taiwan systems. In contrast, unusually wide and deep channels on the Pacific margin of Antarctica and in southeast Greenland suggest additional mechanisms of margin development.

Finally, our **classification for asymmetric channels** provides a framework to connect morphology with underlying controls. Our global analysis confirms that submarine channels exhibit substantial morphometric variability even within the same channel, not only across different settings, underscoring the need for process interpretations that go beyond morphology alone.

CRediT authorship contribution statement

Nadezhda Lagunova: Writing – original draft, Visualization, Software, Methodology. **Tilmann Schwenk:** Writing – review & editing, Validation, Supervision, Conceptualization. **Michael A. Clare:** Writing – review & editing, Validation, Supervision, Conceptualization. **Ricardo Silva Jacinto:** Writing – review & editing, Validation, Supervision, Conceptualization. **Dierk Hebbeln:** Writing – review & editing, Validation, Supervision, Conceptualization. **Volkhard Spieß:** Writing – review & editing, Validation, Conceptualization. **Gerhard Bohrmann:** Writing – review & editing, Validation, Conceptualization. **Pelle H. Adema:** Writing – review & editing, Validation, Conceptualization. **Joris T. Eggenhuisen:** Writing – review & editing, Validation, Conceptualization. **Elda Miramontes:** Writing – review & editing, Validation, Supervision, Resources, Project administration, Funding acquisition, Conceptualization.

Declaration of competing interest

The authors declare the following financial interests/personal relationships which may be considered as potential competing interests: Nadezhda Lagunova reports financial support was provided by German Research Foundation. Elda Miramontes reports financial support was provided by German Research Foundation. Joris Eggenhuisen reports financial support was provided by Dutch Research Council. Pelle Adema reports financial support was provided by Dutch Research Council. If there are other authors, they declare that they have no known competing financial interests or personal relationships that could have appeared to influence the work reported in this paper.

Acknowledgements

We gratefully acknowledge Alice Lefebvre for providing the code employed to extract near-bottom currents from the Copernicus ocean-current model. E. Miramontes and N. Lagunova acknowledge funding by the German Research Foundation (DFG), project number 509877600. P. Adema and J.T. Eggenhuisen were supported by the Dutch Research Council (grant OCENW.KLEIN.462).

Appendix A. Supplementary data

Supplementary data to this article can be found online at https://doi.org/10.1016/j.geomorph.2026.110445.

Data availability

The dataset generated and analysed during this study, containing geomorphic parameters of submarine channels, are accessible at: https://doi.org/10.1594/PANGAEA.988633.

References

Adema, P.H., Eggenhuisen, J.T., Bleeker, J., Jacinto, R.S., Miramontes, E., 2025a. Turbidity current flow structure and its modulation by contour currents: Insights from 3D flume experiments. Mar. Geol. 480, 107469. https://doi.org/10.1016/j.margeo.2024.107469.

Adema, P.H., Eggenhuisen, J.T., Jacinto, R.S., Lagunova, N., Alwadhakhi, A.I., van der Woning, R., Miramontes, E., 2025b. Submarine channel shape controls combined turbidity current–contour current flow. Mar. Geol. 490, 107646. https://doi.org/10.1016/j.margeo.2025.107646.

Allen, C., Peakall, J., Hodgson, D.M., Bradbury, W., Booth, A.D., 2022. Latitudinal changes in submarine channel-levee system evolution, architecture and flow processes. Front. Earth Sci. 10, 976852. https://doi.org/10.3389/feart.2022.976852.

Amy, L.A., Peakall, J., Talling, P.J., 2005. Density- and viscosity-stratified gravity currents: Insight from laboratory experiments and implications for submarine flow deposits. Sediment. Geol. 179, 5–29. https://doi.org/10.1016/j.sedgeo.2005.04.009.

Bailey, L.P., Clare, M.A., Hunt, J.E., Kane, I.A., Miramontes, E., Fonnesu, M., Argiolas, R., Malgesini, G., Wallerand, R., 2024. Highly variable deep-sea currents over tidal and seasonal timescales. Nat. Geosci. 17, 787–794. https://doi.org/10.1038/s41561-024-01494-2.

Bernhardt, A., Melnick, D., Jara-Muñoz, J., Argandoña, B., González, J., Strecker, M.R., 2015. Controls on submarine canyon activity during sea-level highstands: The Biobío canyon system offshore Chile. Geosphere 11, 1226–1255. https://doi.org/10.1130/GES01063.1.

Carter, R.M., Carter, L., 1987. The bounty channel system: A 55-million-year-old sediment conduit to the deep sea, Southwest Pacific Ocean. Geo-Mar. Lett. 7, 183–190. https://doi.org/10.1007/BF02242770.

Carter, L., Carter, R.M., 1988. Late Quaternary development of left-bank-dominant levees in the Bounty Trough, New Zealand. Mar. Geol. 78, 185–197. https://doi.org/10.1016/0025-3227(88)90108-9.

Carter, R.M., Carter, L., 1996. The abyssal bounty fan and lower Bounty Channel: evolution of a rifted-margin sedimentary system. Mar. Geol. 130, 181–202. https://doi.org/10.1016/0025-3227(95)00139-5.

Carter, L., Gavey, R., Talling, P.J., Liu, J.T., 2014. Insights into submarine geohazards from breaks in subsea telecommunication cables. Oceanography 27, 58–67.

Chen, P., Kane, I.A., Clare, M.A., Soutter, E.L., Mienis, F., Wogelius, R.A., Keavney, E., 2025. Direct evidence that microplastics are transported to the deep sea by turbidity currents. Environ. Sci. Technol. 59, 7278–7287. https://doi.org/10.1021/acs.est.4c12007.

Copernicus Marine Service, 2015. Arctic Ocean Physics Analysis and Forecast. Marine Data Store (MDS). 10.48670/MOI-00001.

Copernicus Marine Service, 2016. Global Ocean 1/12° Physics Analysis and Forecast updated Daily. 10.48670/MOI-00016.

Copernicus Marine Service, 2017. Atlantic-Iberian Biscay Irish-Ocean Physics Analysis and Forecast. Marine Data Store (MDS). 10.48670/MOI-00027.

Copernicus Marine Service, 2025. Black Sea Physics Reanalysis. Marine Data Store (MDS). 10.48670/MDS-00356.

Cossu, R., Wells, M.G., Wåhlin, A.K., 2010. Influence of the Coriolis force on the velocity structure of gravity currents in straight submarine channel systems. J. Geophys. Res. Oceans 115. https://doi.org/10.1029/2010JC006208.

Cossu, R., Wells, M.G., Peakall, J., 2015. Latitudinal variations in submarine channel sedimentation patterns: the role of Coriolis forces. J. Geol. Soc. London 172, 161–174. https://doi.org/10.1144/jgs2014-043.

Covault, J.A., Shelef, E., Traer, M., Hubbard, S.M., Romans, B.W., Fildani, A., 2012. Deep-water channel run-out length: insights from seafloor geomorphology. J. Sediment. Res. 82, 21–36. https://doi.org/10.2110/jsr.2012.2.

[software] Čučković, Z., 2025. QGIS Terrain Shading, URL. https://github.com/zoran-cuckovic/QGIS-terrain-shading.

Deng, X., Huang, K., Li, X., 2024. Sedimentary characteristics and evolution of the late Miocene to Quaternary tributary channels in the head of Bounty Channel, New Zealand. Appl. Sci. 14, 6160. https://doi.org/10.3390/app14146160.

Dorrell, R.M., Darby, S.E., Peakall, J., Sumner, E.J., Parsons, D.R., Wynn, R.B., 2013. Superelevation and overspill control secondary flow dynamics in submarine channels. J. Geophys. Res. Oceans 118, 3895–3915. https://doi.org/10.1002/jgrc.20277.

Ercilla, G., Casas, D., Vázquez, J.T., Iglesias, J., Somoza, L., Juan, C., Medialdea, T., León, R., Estrada, F., García-Gil, S., Farran, Marce. lí, Bohoyo, F., García, M., Maestro, A., 2011. Imaging the recent sediment dynamics of the Galicia Bank region (Atlantic, NW Iberian Peninsula). Mar. Geophys. Res. 32, 99–126. https://doi.org/10.1007/s11001-011-9129-x.

[dataset] Escudier, R., Clementi, E., Omar, M., Cipollone, A., Pistoia, J., Aydogdu, A., Drudi, M., Grandi, A., Lyubartsev, V., Lecci, R., Cretí, S., Masina, S., Coppini, G., Pinardi, N., 2020. Mediterranean Sea Physical Reanalysis, 10.25423/CMCC/MEDSEA_MULTIYEAR_PHY_006_004_E3R1.

Fierens, R., Droz, L., Toucanne, S., Raisson, F., Jouet, G., Babonneau, N., Miramontes, E., Landurain, S., Jorry, S.J., 2019. Late Quaternary geomorphology and sedimentary processes in the Zambezi turbidite system (Mozambique Channel). Geomorphology 334, 1–28. https://doi.org/10.1016/j.geomorph.2019.02.033.

Fonnesu, M., Palermo, D., Galbiati, M., Marchesini, M., Bonamini, E., Bendias, D., 2020. A new world-class deep-water play-type, deposited by the syndepositional interaction of turbidity flows and bottom currents: the giant Eocene Coral Field in northern Mozambique. Mar. Pet. Geol. 111, 179–201. https://doi.org/10.1016/j.marpetgeo.2019.07.047.

Fontanier, C., Fabri, M.-C., Buscail, R., Biscara, L., Koho, K., Reichart, G.J., Cossa, D., Galaup, S., Chabaud, G., Pigot, L., 2012. Deep-sea foraminifera from the Cassidaigne Canyon (NW Mediterranean): assessing the environmental impact of bauxite red mud disposal. Mar. Pollut. Bull. 64, 1895–1910. https://doi.org/10.1016/j.marpolbul.2012.06.016.

Fuhrmann, A., Kane, I.A., Clare, M.A., Ferguson, R.A., Schomacker, E., Bonamini, E., Contreras, F.A., 2020. Hybrid turbidite-drift channel complexes: an integrated multiscale model. Geology 48, 562–568. https://doi.org/10.1130/G47179.1.

Gardner, J.V., Armstrong, A.A., Calder, B.R., 2016. Hatteras Transverse Canyon, Hatteras Outer Ridge and environs of the U.S. Atlantic margin: a view from multibeam bathymetry and backscatter. Mar. Geol. 371, 18–32. https://doi.org/10.1016/j.margeo.2015.10.015.

Hansen, L., Janocko, M., Kane, I., Kneller, B., 2017. Submarine channel evolution, terrace development, and preservation of intra-channel thin-bedded turbidites: Mahin and Avon channels, offshore Nigeria. Mar. Geol. 383, 146–167. https://doi.org/10.1016/j.margeo.2016.11.011.

Harris, P.T., Whiteway, T., 2011. Global distribution of large submarine canyons: geomorphic differences between active and passive continental margins. Mar. Geol. 285, 69–86. https://doi.org/10.1016/j.margeo.2011.05.008.

Hasenhündl, M., Blanckaert, K., 2022. A Matlab script for the morphometric analysis of subaerial, subaquatic and extra-terrestrial rivers, channels and canyons. Comput. Geosci. 162, 105080. https://doi.org/10.1016/j.cageo.2022.105080.

Hernández-Molina, F.J., De Castro, S., De Weger, W., Duarte, D., Fonnesu, M., Glazkova, T., Kirby, A., Llave, E., Ng, Z.L., Mantilla Muñoz, O., Rodrigues, S., Rodríguez-Tovar, F.J., Thieblemont, A., Viana, A.R., Yin, S., 2022. Contourites and mixed depositional systems: a paradigm for deepwater sedimentary environments. In: Deepwater Sedimentary Systems. Elsevier, pp. 301–360. https://doi.org/10.1016/B978-0-323-91918-0.00004-9.

Horn, M., Uenzelmann-Neben, G., 2015. The deep western boundary current at the Bounty Trough, east of New Zealand: indications for its activity already before the opening of the Tasmanian Gateway. Mar. Geol. 362, 60–75. https://doi.org/10.1016/j.margeo.2015.01.011.

Imran, J., Parker, G., Pirmez, C., 1999. A nonlinear model of flow in meandering submarine and subaerial channels. J. Fluid Mech. 400, 295–331. https://doi.org/10.1017/S0022112099006515.

Khripounoff, A., Crassous, P., Lo Bue, N., Dennielou, B., Silva Jacinto, R., 2012. Different types of sediment gravity flows detected in the Var submarine canyon (northwestern Mediterranean Sea). Prog. Oceanogr. 106, 138–153. https://doi.org/10.1016/j.pocean.2012.09.001.

Kneller, B., 1995. Beyond the turbidite paradigm: physical models for deposition of turbidites and their implications for reservoir prediction. Geol. Soc. Lond. Spec. Publ. 94, 31–49. https://doi.org/10.1144/GSL.SP.1995.094.01.04.

Kneller, B., Buckee, C., 2000. The structure and fluid mechanics of turbidity currents: a review of some recent studies and their geological implications. Sedimentology 47, 62–94. https://doi.org/10.1046/j.1365-3091.2000.047s1062.x.

Komar, P.D., 1969. The channelized flow of turbidity currents with application to Monterey Deep-Sea Fan Channel. J. Geophys. Res. 74, 4544–4558. https://doi.org/10.1029/JC074i018p04544.

Konsoer, K., Zinger, J., Parker, G., 2013. Bankfull hydraulic geometry of submarine channels created by turbidity currents: relations between bankfull channel characteristics and formative flow discharge. Case Rep. Med. 118, 216–228. https://doi.org/10.1029/2012JF002422.

Kuvaas, B., Kristoffersen, Y., Guseva, J., Leitchenkov, G., Gandjukhin, V., Løvås, O., Sand, M., Brekke, H., 2005. Interplay of turbidite and contourite deposition along the Cosmonaut Sea/Enderby Land margin, East Antarctica. Mar. Geol. 217, 143–159. https://doi.org/10.1016/j.margeo.2005.02.025.

[software] Lagunova, N., 2026. Submarine Channels Morphometry. https://doi.org/10.5281/ZENODO.18876684.

Lewis, K.B., Collot, J., Lallem, S.E., 1998. The dammed Hikurangi Trough: a channel-fed trench blocked by subducting seamounts and their wake avalanches (New Zealand–France GeodyNZ Project). Basin Res. 10, 441–468. https://doi.org/10.1046/j.1365-2117.1998.00080.x.

Li, W., Li, S., Alves, T.M., Rebesco, M., Feng, Y., 2021. The role of sediment gravity flows on the morphological development of a large submarine canyon (Taiwan Canyon), north-east South China Sea. Sedimentology 68, 1091–1108. https://doi.org/10.1111/sed.12818.

Marchès, E., Mulder, T., Cremer, M., Bonnel, C., Hanquiez, V., Gonthier, E., Lecroart, P., 2007. Contourite drift construction influenced by capture of Mediterranean Outflow Water deep-sea current by the Portimão submarine canyon (Gulf of Cadiz, South Portugal). Mar. Geol. 242, 247–260. https://doi.org/10.1016/j.margeo.2007.03.013.

Marchès, E., Mulder, T., Gonthier, E., Cremer, M., Hanquiez, V., Garlan, T., Lecroart, P., 2010. Perched lobe formation in the Gulf of Cadiz: interactions between gravity processes and contour currents (Algarve Margin, Southern Portugal). Sediment. Geol. 229, 81–94. https://doi.org/10.1016/j.sedgeo.2009.03.008.

Mas, V., Mulder, T., Dennielou, B., Schmidt, S., Khripounoff, A., Savoye, B., 2010. Multiscale spatio-temporal variability of sedimentary deposits in the Var turbidite system (North-Western Mediterranean Sea). Mar. Geol. 275, 37–52. https://doi.org/10.1016/j.margeo.2010.04.006.

Migeon, S., Savoye, B., Faugeres, J.-C., 2000. Quaternary development of migrating sediment waves in the Var deep-sea fan: distribution, growth pattern, and implication for levee evolution. Sediment. Geol. 133, 265–293. https://doi.org/10.1016/S0037-0738(00)00043-9.

Miramontes, E., Penven, P., Fierens, R., Droz, L., Toucanne, S., Jorry, S.J., Jouet, G., Pastor, L., Silva Jacinto, R., Gaillot, A., Giraudeau, J., Raisson, F., 2019. The influence of bottom currents on the Zambezi Valley morphology (Mozambique Channel, SW Indian Ocean): in situ current observations and hydrodynamic modelling. Mar. Geol. 410, 42–55. https://doi.org/10.1016/j.margeo.2019.01.002.

Miramontes, E., Eggenhuisen, J.T., Jacinto, R.S., Poneti, G., Pohl, F., Normandeau, A., Campbell, D.C., Hernández-Molina, F.J., 2020. Channel-levee evolution in combined contour current–turbidity current flows from flume-tank experiments. Geology 48, 353–357. https://doi.org/10.1130/G47111.1.

Miramontes, E., Thiéblemont, A., Babonneau, N., Penven, P., Raisson, F., Droz, L., Jorry, S.J., Fierens, R., Counts, J.W., Wilckens, H., Cattaneo, A., Jouet, G., 2021. Contourite and mixed turbidite-contourite systems in the Mozambique Channel (SW Indian Ocean): link between geometry, sediment characteristics and modelled bottom currents. Mar. Geol. 437, 106502. https://doi.org/10.1016/j.margeo.2021.106502.

Mohrig, D., Buttles, J., 2007. Deep turbidity currents in shallow channels. Geology 35, 155. https://doi.org/10.1130/G22716A.1.

Mulder, T., Lecroart, P., Hanquiez, V., Marches, E., Gonthier, E., Guedes, J.-C., Thiébot, E., Jaaidi, B., Kenyon, N., Voisset, M., Perez, C., Sayago, M., Fuchey, Y., Bujan, S., 2006. The western part of the Gulf of Cadiz: contour currents and turbidity currents interactions. Geo-Mar. Lett. 26, 31–41. https://doi.org/10.1007/s00367-005-0013-z.

Mulder, T., Faugères, J.-C., Gonthier, E., 2008. Chapter 21 mixed turbidite–contourite systems. In: Developments in Sedimentology. Elsevier, pp. 435–456. https://doi.org/10.1016/S0070-4571(08)10021-8.

Nanson, R., Arosio, R., Gafeira, J., McNeil, M., Dove, D., Bjarnadóttir, L.R., Dolan, M.F.J., Post, A., Nichol, S., Huang, Z., Guinan, J., Bialik, O.M., Webb, J., Wells, J., Carroll, A. G., 2026. Coastal to deep-marine geomorphic classification: a standardised framework and review of terms to support globally consistent mapping. Earth Sci. Rev. 276, 105439. https://doi.org/10.1016/j.earscirev.2026.105439.

Neil, H., Orpin, A., Nodder, S., Mitchell, J., Northcote, L., Mackay, K., Kane, T., 2015. Large Canyon-Channel Complexes from South Island of New Zealand Show Contrasting Morphologies. AAPG Asia Pac. Reg. Geosci. Technol. Workshop Mod. DepositionalSystems Analog. Pet. Reserv. April 21–22 2015 Wellingt. N. Z. https://www.searchanddiscovery.com/abstracts/pdf/2015/90235gtw/abstracts/ndx_neil.pdf.

Normandeau, A., Campbell, D.C., Cartigny, M.J.B., 2019. The influence of turbidity currents and contour currents on the distribution of deep-water sediment waves offshore eastern Canada. Sedimentology 66, 1746–1767. https://doi.org/10.1111/sed.12557.

Palm, F.A., Peakall, J., Hodgson, D.M., Marsset, T., Silva Jacinto, R., Dennielou, B., Babonneau, N., Wright, T.J., 2021. Width variation around submarine channel bends: Implications for sedimentation and channel evolution. Mar. Geol. 437, 106504. https://doi.org/10.1016/j.margeo.2021.106504.

Payo Payo, M., 2016. Modélisation du transport sédimentaire et des interactions morphodynamiques par les courants de turbidité dans les canyons sous-marins. Application à la Méditerranée Occidentale. PhD thesis. Université de Bretagne occidentale, Brest. Available at: https://archimer.ifremer.fr/doc/00498/60919/.

Peakall, J., Kane, I.A., Masson, D.G., Keevil, G., McCaffrey, W., Corney, R., 2012. Global (latitudinal) variation in submarine channel sinuosity. Geology 40, 11–14. https://doi.org/10.1130/G32295.1.

Peakall, J., Wells, M.G., Cossu, R., Kane, I.A., Masson, D.G., Keevil, G.M., McCaffrey, W., Corney, R., 2013. Global (latitudinal) variation in submarine channel sinuosity: REPLY. Geology 41, e288. https://doi.org/10.1130/G34319Y.1.

Popescu, I., Lericolais, G., Panin, N., Wong, H.K., Droz, L., 2001. Late Quaternary channel avulsions on the Danube deep-sea fan, Black Sea. Mar. Geol. 179, 25–37. https://doi.org/10.1016/S0025-3227(01)00197-9.

Rasmussen, S., Lykke-Andersen, H., Kuijpers, A., Troelstra, S.R., 2003. Post-Miocene sedimentation at the continental rise of Southeast Greenland: the interplay between turbidity and contour currents. Mar. Geol. 196, 37–52. https://doi.org/10.1016/S0025-3227(03)00043-4.

Rebesco, M., Larter, R.D., Camerlenghi, A., Barker, P.F., 1996. Giant sediment drifts on the continental rise west of the Antarctic Peninsula. Geo-Mar. Lett. 16, 65–75. https://doi.org/10.1007/BF02202600.

Rebesco, M., Hernández-Molina, F.J., Van Rooij, D., Wåhlin, A., 2014. Contourites and associated sediments controlled by deep-water circulation processes: state-of-the-art and future considerations. Mar. Geol. 352, 111–154. https://doi.org/10.1016/j.margeo.2014.03.011.

Reimchen, A.P., Hubbard, S.M., Stright, L., Romans, B.W., 2016. Using sea-floor morphometrics to constrain stratigraphic models of sinuous submarine channel systems. Mar. Pet. Geol. 77, 92–115. https://doi.org/10.1016/j.marpetgeo.2016.06.003.

Rodrigues, Hernández-Molina, F.J., Larter, R.D., Rebesco, M., Hillenbrand, C.-D., Lucchi, R.G., Rodríguez-Tovar, F.J., 2022a. Sedimentary model for mixed depositional systems along the Pacific margin of the Antarctic Peninsula: decoding the interplay of deep-water processes. Mar. Geol. 445, 106754. https://doi.org/10.1016/j.margeo.2022.106754.

Rodrigues, S., Hernández-Molina, F.J., Fonnesu, M., Miramontes, E., Rebesco, M., Campbell, D.C., 2022b. A new classification system for mixed (turbidite-contourite) depositional systems: examples, conceptual models and diagnostic criteria for modern and ancient records. Earth Sci. Rev. 230, 104030. https://doi.org/10.1016/j.earscirev.2022.104030.

Savitzky, A.G.M.J.E., 1964. Smoothing and differentiation of data by simplified least squares procedures. Anal. Chem. 36, 1627–1639.

Shumaker, L.E., Jobe, Z.R., Johnstone, S.A., Pettinga, L.A., Cai, D., Moody, J.D., 2018. Controls on submarine channel-modifying processes identified through morphometric scaling relationships. Geosphere 14, 2171–2187. https://doi.org/10.1130/GES01674.1.

Stanev, E., 2005. Understanding Black Sea dynamics: overview of recent numerical modeling. Oceanography 18, 56–75. https://doi.org/10.5670/oceanog.2005.42.

Stevenson, C.J., Talling, P.J., Wynn, R.B., Masson, D.G., Hunt, J.E., Frenz, M., Akhmetzhanhov, A., Cronin, B.T., 2013. The flows that left no trace: very large-volume turbidity currents that bypassed sediment through submarine channels without eroding the sea floor. Mar. Pet. Geol. 41, 186–205. https://doi.org/10.1016/j.marpetgeo.2012.02.008.

Sylvester, Z., Pirmez, C., 2019. Latitudinal changes in the morphology of submarine channels: reevaluating the evidence for the influence of the coriolis force. In: Fraticelli, C.M. (Ed.), Latitudinal Controls on Stratigraphic Models and Sedimentary Concepts. SEPM (Society for Sedimentary Geology), pp. 82–92. https://doi.org/10.2110/sepmsp.108.02.

Sylvester, Z., Pirmez, C., Cantelli, A., Jobe, Z.R., 2013. Global (latitudinal) variation in submarine channel sinuosity: COMMENT. Geology 41, e287. https://doi.org/10.1130/G33548C.1.

Talling, P.J., 2014. On the triggers, resulting flow types and frequencies of subaqueous sediment density flows in different settings. Mar. Geol. 352, 155–182. https://doi.org/10.1016/j.margeo.2014.02.006.

Talling, P.J., Hage, S., Baker, M.L., Bianchi, T.S., Hilton, R.G., Maier, K.L., 2024. The global turbidity current pump and its implications for organic carbon cycling. Ann. Rev. Mar. Sci. 16, 105–133. https://doi.org/10.1146/annurev-marine-032223-103626.

[software] Virtanen, P., Gommers, R., Oliphant, T.E., Haberland, M., Reddy, T., Cournapeau, D., Burovski, E., Peterson, P., Weckesser, W., Bright, J., Van Der Walt, S.J., Brett, M., Wilson, J., Millman, K.J., Mayorov, N., Nelson, A.R.J., Jones, E., Kern, R., Larson, E., Carey, C.J., Polat, İ., Feng, Y., Moore, E.W., VanderPlas, J., Laxalde, D., Perktold, J., Cimrman, R., Henriksen, I., Quintero, E.A., Harris, C.R., Archibald, A.M., Ribeiro, A.H., Pedregosa, F., Van Mulbregt, P., SciPy 1.0 Contributors, Vijaykumar, A., Bardelli, A.P., Rothberg, A., Hilboll, A., Kloeckner, A., Scopatz, A., Lee, A., Rokem, A., Woods, C.N., Fulton, C., Masson, C., Häggström, C., Fitzgerald, C., Nicholson, D.A., Hagen, D.R., Pasechnik, D.V., Olivetti, E., Martin, E., Wieser, E., Silva, F., Lenders, F., Wilhelm, F., Young, G., Price, G.A., Ingold, G.-L., Allen, G.E., Lee, G.R., Audren, H., Probst, I., Dietrich, J.P., Silterra, J., Webber, J.T., Slavič, J., Nothman, J., Buchner, J., Kulick, J., Schönberger, J.L., De Miranda Cardoso, J.V., Reimer, J., Harrington, J., Rodríguez, J.L.C., Nunez-Iglesias, J., Kuczynski, J., Tritz, K., Thoma, M., Newville, M., Kümmerer, M., Bolingbroke, M., Tartre, M., Pak, M., Smith, N.J., Nowaczyk, N., Shebanov, N., Pavlyk, O., Brodtkorb, P.A., Lee, P., McGibbon, R.T., Feldbauer, R., Lewis, S., Tygier, S., Sievert, S., Vigna, S., Peterson, S., More, S., Pudlik, T., Oshima, T., Pingel, T.J., Robitaille, T.P., Spura, T., Jones, T.R., Cera, T., Leslie, T., Zito, T., Krauss, T., Upadhyay, U., Halchenko, Y.O., Vázquez-Baeza, Y., 2020. SciPy 1.0: fundamental algorithms for scientific computing in Python. Nat. Methods 17, 261–272. https://doi.org/10.1038/s41592-019-0686-2.

Warnke, F., Schwenk, T., Miramontes, E., Spieß, V., Wenau, S., Bozzano, G., Baqués, M., Kasten, S., 2023. Multibeam Bathymetry Processed Data (Kongsberg EM122 Working Area Dataset) of RV SONNE During Cruise SO260/1. Argentine Continental Margin. https://doi.org/10.1594/PANGAEA.938459.

Warratz, G., Schwenk, T., Voigt, I., Bozzano, G., Henrich, R., Violante, R., Lantzsch, H., 2019. Interaction of a deep-sea current with a blind submarine canyon (Mar del Plata Canyon, Argentina). Mar. Geol. 417, 106002. https://doi.org/10.1016/j.margeo.2019.106002.

Weiss, A., 2001. Topographic position and landforms analysis. Presented at the ESRI user conference, San Diego, CA. https://www.jennessent.com/downloads/TPI-poster-TNC_18x22.pdf.

Wells, M., Cossu, R., 2013. The possible role of Coriolis forces in structuring large-scale sinuous patterns of submarine channel–levee systems. Philos. Trans. R. Soc. A Math. Phys. Eng. Sci. 371, 20120366. https://doi.org/10.1098/rsta.2012.0366.

Wilckens, H., Miramontes, E., Schwenk, T., Artana, C., Zhang, W., Piola, A.R., Baques, M., Provost, C., Hernández-Molina, F.J., Felgendreher, M., Spieß, V., Kasten, S., 2021. The erosive power of the Malvinas Current: Influence of bottom currents on morpho-sedimentary features along the northern Argentine margin (SW Atlantic Ocean). Mar. Geol. 439, 106539. https://doi.org/10.1016/j.margeo.2021.106539.

[dataset] Wintersteller, P., Klaucke, I., 2016. Gridded Bathymetry From Multibeam Echosounder EM122 Data of the Cruise MSM34/1 (2013). doi:https://doi.org/10.1594/PANGAEA.860483.

Wintersteller, P., Kramer, L., 2019. Gridded Bathymetry From EM122 Multibeam Echosounder of RV Sonne Cruise SO266 (Offshore SW Taiwan). https://doi.org/10.1594/PANGAEA.900980.

Wynn, R.B., Cronin, B.T., Peakall, J., 2007. Sinuous deep-water channels: genesis, geometry and architecture. Mar. Pet. Geol. 24, 341–387. https://doi.org/10.1016/j.marpetgeo.2007.06.001.

Xu, S., Wang, Y., Peng, X., Zou, H., Qiu, Y., Gong, C., Zhuo, H., 2014. Origin of Taiwan Canyon and its effects on deepwater sediment. Sci. China Earth Sci. 57, 2769–2780. https://doi.org/10.1007/s11430-014-4942-0.

Zhang, R., Tian, D., Li, X., Aziz, T., Wu, J., Jiang, T., Lu, G., Xie, X., 2026. Channel confinement drives unidirectional migration: coupling of flow structure and sedimentary evolution in combined turbidity–bottom current flows. J. Mar. Sci. Eng. 14, 152. https://doi.org/10.3390/jmse14020152.